


 Cite this: *RSC Adv.*, 2022, **12**, 25240

 Received 12th July 2022
 Accepted 23rd August 2022

DOI: 10.1039/d2ra04301g

rsc.li/rsc-advances

Review of the application of Cu-containing SSZ-13 in NH₃-SCR-DeNO_x and NH₃-SCO

 Magdalena Jabłońska *

The reduction of NO_x emissions has become one of the most important subjects in environmental protection. Cu-containing SSZ-13 is currently the state-of-the-art catalyst for the selective catalytic reduction of NO_x with ammonia (NH₃-SCR-DeNO_x). Although the current-generation catalysts reveal enhanced activity and remarkable hydrothermal stability, still open challenges appear. Thus, this review focuses on the progress of Cu-containing SSZ-13 regarding preparation methods, hydrothermal resistance and poisoning as well as reaction mechanisms in NH₃-SCR-DeNO_x. Remarkably, the paper reviews also the progress of Cu-containing SSZ-13 in the selective ammonia oxidation into nitrogen and water vapor (NH₃-SCO). The dynamics in the NH₃-SCR-DeNO_x and NH₃-SCO fields make this review timely.

Introduction

Nitrogen oxides (NO_x, consisting of >95% NO and <5% NO₂) are one of the major atmospheric pollutant gasses emitted from vehicle engines (*e.g.*, automobiles, ships, *etc.*) and industrial boiler processes. NO_x are formed *via* different mechanisms such as thermal-NO_x, prompt-NO_x and fuel-NO_x.^{1,2} Nitrogen oxides affect human health (*e.g.*, lowering the body's resistance to bacterial infections, eye and respiratory system irritation, causing problems with breathing, allergic diseases, *etc.*). Furthermore, the hazards of NO_x include the promotion of

global warming and the formation of photochemical smog, acid rain, atmospheric haze (fine particle pollution) and ozone depletion, while the control of NO_x emission remains a challenging task in the field of environmental catalysis.¹⁻⁴ The upcoming EU emission legislation challenges researchers and engineers to keep the NO_x emissions at a very low level under various boundary conditions. The selective catalytic reduction with ammonia (NH₃-SCR-DeNO_x: 4NH₃ + 4NO + O₂ → 4N₂ + 6H₂O) is one of the most effective technologies for removing NO_x from diesel engine exhausts with an 80–95% removal efficiency.^{1,2} Catalysts – typically metal-oxides, noble metals, metal exchanged zeolites or hybrid systems – are an integral part of NH₃-SCR-DeNO_x.⁵⁻⁷ Much research has been done on Cu-containing ZSM-5 catalysts since its discovery in 1986 by Iwamoto *et al.*⁸ However, Cu-containing ZSM-5, beta or SAPO-34 suffer from poor hydrothermal stability.^{9,10} Cu-containing SSZ-13 (standard oil synthetic zeolite-thirteen, chabazite (CHA)-type zeolite) catalysts have been commercialized in the US and Europe since 2010 due to their efficient reduction of NO_x and enhanced hydrothermal stability.^{11,12} The CHA framework is composed of four-, six-, and eight-membered rings arranged to form a tridimensional system of channels perpendicular to each other (0.38 × 0.38 nm; *R3m* (#166) space group).^{13,14} Examples of morphology of SSZ-13 are given in Fig. 1a. SSZ-13 was first synthesized by Zones in 1985¹⁵ applying the very costly template *N,N,N*-trimethyl-1-adamantammonium hydroxide (TMAdaOH). Nowadays, SSZ-13 can be synthesized by applying a variety of cheaper templates, including choline chloride,^{16,17} *N,N,N*-dimethylethylcyclohexylammonium bromide (DMCHABr),¹⁸ *etc.* Cu-SSZ-13 prepared *via* ion-exchange showed improved activity and N₂ selectivity (*i.e.*, lower amounts of NO_x by-products) compared to Cu-ZSM-5 and Cu-beta (Fig. 1b).¹¹ The activity of catalysts was maintained even

Institute of Chemical Technology, Universität Leipzig, Linnéstr. 3, 04103 Leipzig, Germany. E-mail: magdalena.jablonska@uni-leipzig.de



Magdalena Jabłońska received her PhD (2014) degree from the Faculty of Chemistry of Jagiellonian University in Kraków under the supervision of Prof. Lucjan Chmielarz; and Eng. (2013) from the Faculty of Energy and Fuel of the University of Science and Technology (AGH) under supervision of Prof. Teresa Grzybek. Afterwards, she joined the group of Prof. Regina Palkovits at RWTH Aachen University as

postdoctoral fellow (2014–2017). Since 2017, she is a Junior Group Leader at Leipzig University, Germany. Her research focusses on environmental catalysis, specifically on diesel aftertreatment systems.



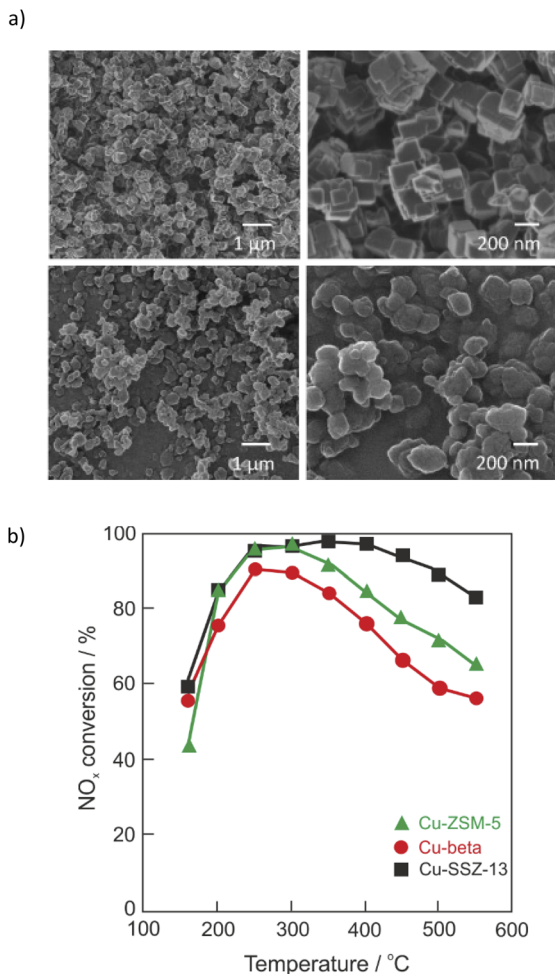


Fig. 1 (a) Examples of helium ion microscopy (HIM) images of SSZ-13. Reproduced from ref. 14 with permission from Elsevier, copyright 2017; (b) NO_x conversion over Cu-SSZ-13 (squares), Cu-beta (circles), and Cu-ZSM-5 (triangles). Reproduced from ref. 11 with permission from Elsevier, copyright 2010.

after severe hydrothermal treatment at 800 °C for 16 h.^{11,19–21} Still, some challenges remain for Cu-containing SSZ-13, including broadening the reaction temperature window together with improved (thermal) stability against chemical poisons. Although some review articles on the Cu-containing SSZ-13 were already published in 2015–2021,^{22–27} extensive studies on the Cu-containing SSZ-13 catalysts concerning preparations methods, hydrothermal stability and poisoning, the reaction mechanisms as well as the determination of active sites are of great interest. Thus, all these factors constitute the present review, which covers the thorough literature of the last ten years. However, this review did not include patents.

Preparation methods of Cu-containing SSZ-13

Kwak *et al.*²⁸ first suggested the presence of two different cationic Cu sites in Cu-SSZ-13, while Giordanino *et al.*²⁹ first reported the presence of [Cu(OH)]⁺ species in Cu-SSZ-13. Cu-

containing SSZ-13 contains two active sites for NH₃-SCR-DeNO_x, Cu²⁺ in double-six-membered ring (D6R) cages and [Cu(OH)]⁺ in CHA cages, which are balanced by a pair of negative charges (2Z) and a single framework negative charge (Z), respectively^{30–32} (Fig. 2a). The concentration of [Cu(OH)]⁺ ions within the eight-ring windows of Cu-SSZ-13 increases as the $n(\text{Cu})/n(\text{Al})$ ratio rises, unlike that of Cu²⁺ ions on D6Rs.³³ The dehydration of the [Cu(OH)]⁺ ions may lead to the formation of Cu⁺ species ([Cu(OH)]⁺ → Cu⁺ + HO⁻),³⁴ or [Cu–O–Cu]²⁺ oxocations (–Al–O–Cu²⁺–OH + –Al–O–Cu²⁺–OH → –Al–O–[Cu–O–Cu]²⁺–O–Al– + H₂O).³⁵ Furthermore, Verma *et al.*^{36,37} suggested that when the $n(\text{Cu})/n(\text{Al})$ is above 0.2, Cu_xO_y are also present. Such aggregated copper oxide species catalyze ammonia oxidation.³⁸ Fickel and Lobo¹² pioneered in the investigation over Cu species in Cu-SSZ-13 with low $n(\text{Si})/n(\text{Al})$ and 4.39 wt% of Cu. They proposed that the Cu cations exist exclusively in the form of isolated Cu²⁺ ions and are located in the cages coordinated with three oxygen atoms of the six-membered rings (6MRs). Nowadays it is recognized that the location, as well as the nature of the Cu cations, varies significantly depending on the $n(\text{Si})/n(\text{Al})$ ratio and also on the Cu loading. Thus, the copper species can occupy four types of cationic sites in CHA, such as site I – displaced from the six-membered-ring into the ellipsoidal cavity, site II – located near the center of the ellipsoidal cavity, site III – located in the center of the hexagonal prism, and site IV – located near the eight-membered-ring window.^{39,40} The copper species can be introduced into the CHA structure *via* different techniques, including ion-exchange, one-pot hydrothermal method, solid-state ion-exchange, *etc.* Table 1 summarizes the catalyst preparation, reaction conditions, and NO_x conversion in NH₃-SCR-DeNO_x above 80% and related by-products in the range. The activity and selectivity of the Cu-containing systems depend on multiple factors, particularly catalyst composition (*e.g.*, $n(\text{Si})/n(\text{Al})$ ratio and copper species loading) and treatment history (*e.g.*, degreening and hydrothermal ageing). It is important to note that the reaction conditions are generally different from each other, including the feed gas composition, total flow, catalyst dosage, and even measurement systems. Therefore, it is hard to compare the activity of the various catalysts in detail. However, a rough comparison is still feasible. Other transition metals have been introduced to improve the activity of catalysts (*e.g.*, Fe,^{41–44} Mn,^{45,46} *etc.*). In the current review, the focus is given mainly on the Cu-containing SSZ-13.

Ion-exchange

In the most widely applied preparation method reported in the literature – ion-exchange, the initial Na-SSZ-13 must also be ion-exchanged with NH₄NO₃ and Cu²⁺ salt solutions to obtain Cu-SSZ-13. The NH₄⁺-form has been reported to improve the mobility of Cu²⁺ ions and promote the ion-exchange rates and levels.⁴⁷ However, the ion-exchange properties (thus, the nature and location of copper species) are influenced by the synthesis conditions of SSZ-13, such as silica source, aluminium source, $n(\text{Si})/n(\text{Al})$ ratio, organic structure-directing agent, water content, alkalinity, ageing time, crystallization temperature or



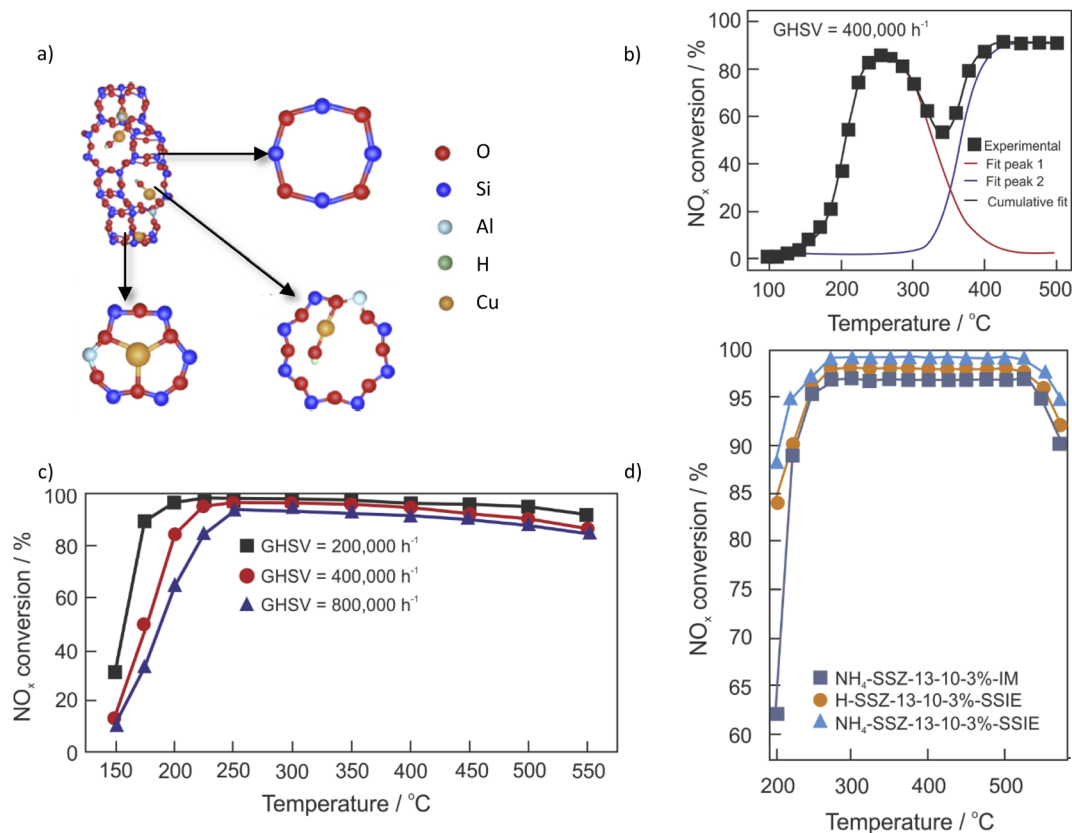


Fig. 2 (a) The structure of Cu-SSZ-13, which contains four-membered, six-membered, and eight-membered rings. Reproduced from ref. 30 with permission from Elsevier, copyright 2022; (b) NO_x conversion (■) over Cu-SSZ-13 with $n(\text{Si})/n(\text{Al}) = 12$ and $n(\text{Cu})/n(\text{Al}) = 0.13$. Also included are simulated curves assuming low- and high-temperature reaction routes. Reproduced from ref. 51 with permission from ACS Publications, copyright 2017; (c) NO_x conversion over (3.8 wt%)Cu-SSZ-13 under different GHSVs. Reproduced from ref. 67 with permission from ACS Publications, copyright 2014; (d) NO_x conversion over Cu-SSZ-13 prepared via solid-state ion-exchange (SSIE) and impregnation (IM). Reproduced from ref. 47 with permission from Elsevier, copyright 2022.

time,^{48–50} etc. Furthermore, ion-exchange variables such as the copper precursor, temperature and time are also influencing factors. For example, Gao *et al.*⁴⁹ prepared SSZ-13 with different $n(\text{Si})/n(\text{Al})$ ratios (6, 12 and 35) by the traditional synthesis method with N,N,N -trimethyl-1-adamantammonium hydroxide as a structure-directing agent. They proposed that the location of Cu^{2+} ions and their redox properties can be adjusted through the variation of the $n(\text{Si})/n(\text{Al})$ ratio of Cu-SSZ-13. Moreover, the isolated Cu^{2+} ions in Cu-SSZ-13 are adjusted by the application of different Cu precursors,³⁰ *i.e.*, in 6MRs for the catalysts prepared with CuCl_2 and $\text{Cu}(\text{CH}_3\text{COO})_2$ precursors and in 8MRs for the catalysts prepared with $\text{Cu}(\text{NO}_3)_2$ and CuSO_4 precursors. The presence of catalytic centers with different activities can be visualized via the seagull profile, *i.e.*, first, an increase in NO conversion with temperature, followed by a decrease in conversion at intermediate temperatures (*ca.* 250–350 °C), and finally an increase again at higher temperatures^{51,52} (Fig. 2b). The seagull profile is often seen for Cu-SSZ-13 with low Cu content (*i.e.*, 0.5–3 wt%),^{53,54} NH_3 -SCR-DeNO_x with high space velocity, low oxygen concentration (*e.g.*, 2 vol%) as well as in the presence of hydrocarbons.⁵²

The ion-exchange properties can also be varied for the micro-/mesoporous materials.^{55–57} In the case of SSZ-13,⁵⁸ mesopores with diameters of 2–10 nm were introduced into the zeolite H-SSZ-13 after treatment with NaOH. Cu-containing SSZ-13 with the support treated with an aqueous solution of 0.1 M NaOH showed enhanced activity in NH_3 -SCR-DeNO_x. The use of higher concentrations of NaOH led to a drop in activity. Moreover, lower activity was also reported for the steamed Cu-SSZ-13. Further studies⁵⁹ proved Cu-containing SSZ-13, with the support treated with 0.1 M aqueous solution to be the most active catalyst in the series (0–0.3 M concentration of NaOH solution). The copper species loading introduced via ion-exchange was comparable for the catalysts with unmodified and post-modified support; however, they varied significantly between both studies. As can be seen from Table 1, pos. 12–50, the amount of introduced copper species varies significantly among the samples, *i.e.*, it is uncontrollable. Furthermore, as the ion-exchange requires successive washing, filtering, drying, calcining and solute recycling procedures, many researchers turn to alternative preparation procedures, *e.g.*, the one-pot hydrothermal method.



Table 1 Representative results of NH_3 -SCR-DeNO_x over Cu-containing SSZ-13 reported in the literature

Pos.	Sample	Preparation method	Reaction conditions	Operation temperature for achieving > 80% NO _x conversion/ ^o C ((by-)product formation)	Ref.
1	(1.4 wt%)Cu-SSZ-13 ($n(\text{Si})/n(\text{Al}) = 4.8$) monolith catalyst	Commercial; degreening: 14 vol% O ₂ , 5 vol% H ₂ O, 5 vol% CO ₂ , N ₂ balance, 600 °C, 4 h	0.035 vol% NO, 0.035 vol% NH ₃ , 14 vol% O ₂ , 5 vol% CO ₂ , 5 vol% H ₂ O, N ₂ balance, GHSV 30,000 h ⁻¹	200–500 (<7% N ₂ O selectivity)	68
2	(1.63 wt%)Cu-SSZ-13 ($n(\text{Si})/n(\text{Al}) = 16$) monolith catalyst	Commercial; degreening: 10 vol% O ₂ , 7 vol% H ₂ O, 8 vol% CO ₂ , N ₂ balance, 650 °C, 4 h; *hydrothermal treatment: 10 vol% H ₂ O, 18.9 vol% O ₂ , N ₂ balance, 650 °C, 100 h	0.05 vol% NO, 0.05 vol% NH ₃ , 7 vol% H ₂ O, 8 vol% CO ₂ , 10 vol% O ₂ , N ₂ balance, GHSV 60,000 h ⁻¹	200–500 (not shown), *200–500 (not shown)	69
3	(1.63 wt%)Cu-SSZ-13 ($n(\text{Si})/n(\text{Al}) = 16$) monolith catalyst	Commercial; degreening: 10 vol% O ₂ , 7 vol% H ₂ O, 8 vol% CO ₂ , N ₂ balance, 650 °C, 50 h	0.05 vol% NO, 0.05 vol% NH ₃ , 7 vol% H ₂ O, 8 vol% CO ₂ , 10 vol% O ₂ , N ₂ balance, GHSV 60,000 h ⁻¹	200–500 (<15 ppm N ₂ O)	70
4	(2.2 wt%)Cu-SSZ-13 ($n(\text{Si})/n(\text{Al}) = 13.6$) monolith catalyst	Commercial; *hydrothermal treatment: 10 vol% H ₂ O, air balance, 800 °C, 12 h	0.1 vol% NO, 0.11 vol% NH ₃ , 5 vol% O ₂ , 10 vol% H ₂ O, N ₂ balance, GHSV 30,000 h ⁻¹	225–550 (not shown) *225–575 (not shown)	71
5	(2.4 wt%)Cu-SSZ-13 ($n(\text{Si})/n(\text{Al}) = 15$) monolith catalyst	Commercial; degreening: 10 vol% O ₂ , 7 vol% H ₂ O, 8 vol% CO ₂ , Ar balance, 550 °C, 4 h	0.02 vol% NO, 0.02 vol% NH ₃ , 5 vol% O ₂ , 5 vol% H ₂ O, Ar balance, GHSV 40,000 h ⁻¹	200–450 (<6% NO ₂ , N ₂ O concentration)	72
6	(2.7 wt%)Cu-SSZ-13 ($n(\text{Si})/n(\text{Al}) = 12$) monolith catalyst	Commercial; degreening: 10 vol% H ₂ O, air balance, 650 °C, 12 h; *hydrothermal treatment: 10 vol% H ₂ O, air balance, 800 °C, 16 h; pre-treatment: 21 vol% O ₂ , N ₂ balance, 600 °C, 20 min	0.05 vol% NO, 0.05 vol% NH ₃ , 5 vol% O ₂ , 3 vol% H ₂ O, N ₂ balance, GHSV 120,000 h ⁻¹	200–600 (<10 ppm N ₂ O), *200–500 (<10 ppm N ₂ O)	73
7	(2.8 wt%)Cu-SSZ-13 ($n(\text{Si})/n(\text{Al}) = 35$) monolith catalyst	Commercial; calcination, 450 °C, 0.5 h; 12.5 vol% H ₂ O, air balance, 800 °C, 16 h	0.02 vol% NO, 0.02 vol% NH ₃ , 10 vol% O ₂ , 5 vol% H ₂ O, 8 vol% CO ₂ , N ₂ balance, GHSV 30,000 h ⁻¹	250–450 (not shown)	21
8	(3 wt%)Cu-SSZ-13 ($n(\text{Si})/n(\text{Al}) = 7$) monolith catalyst	Commercial; degreening: 10 vol% O ₂ , 5 vol% H ₂ O, N ₂ balance, 500 °C, 1 h	0.1 vol% NO, 0.1 vol% NH ₃ , 10 vol% O ₂ , 5 vol% H ₂ O, N ₂ balance, GHSV 120,000 h ⁻¹	200–500 (<15 ppm N ₂ O)	52
9	Cu-SSZ-13 (Cu content, $n(\text{Si})/n(\text{Al})$ not shown) monolith catalyst	Commercial; degreening: 10 vol% O ₂ , 7 vol% H ₂ O, 8 vol% CO ₂ , N ₂ balance, 550–600 °C, 4 h	0.02 vol% NO, 0.02 vol% NH ₃ , 10 vol% O ₂ , 5 vol% H ₂ O, Ar balance, GHSV 40,000 h ⁻¹	200–500 (not shown)	74
10	Cu-SSZ-13 (Cu content, $n(\text{Si})/n(\text{Al})$ not shown) monolith catalyst	Commercial; hydrothermal treatment: 10 vol% O ₂ , 8 vol% CO ₂ , 7 vol% H ₂ O, N ₂ balance, 800 °C, 4 h	0.02 vol% NO, 0.02 vol% NH ₃ , 10 vol% O ₂ , 8 vol% CO ₂ , 7 vol% H ₂ O, N ₂ balance, GHSV 40,000 h ⁻¹	200–500 (not shown)	75
11	Cu-SSZ-13 (Cu content, $n(\text{Si})/n(\text{Al})$ not shown) monolith catalyst	Commercial; hydrothermal treatment: 14 vol% O ₂ , 5 vol% CO ₂ , 5 vol% H ₂ O, N ₂ balance, 750 °C, 16 h	0.035 vol% NO, 0.035 vol% NH ₃ , 14 vol% O ₂ , 2 vol% H ₂ O, N ₂ balance, GHSV 140,000 h ⁻¹	250–500 (not shown)	76
Ion-exchange					
12	Cu-SSZ-13 ($n(\text{Si})/n(\text{Al}) = 6$) (Cu content not shown)	Ion-exchange, calcination, 500 °C, 2 h, air	0.035 vol% NO, 0.035 vol% NH ₃ , 14 vol% O ₂ , 2 vol% H ₂ O, N ₂ balance, GHSV 30,000 h ⁻¹	200–550 (<10 ppm NO ₂ formation, <5 ppm N ₂ O formation)	11
13	(0.87 wt%)Cu-SSZ-13 ($n(\text{Si})/n(\text{Al}) = 6$)	Ion-exchange, calcination, 550 °C, 8 h, air; **hydrothermal treatment: 10 vol% H ₂ O, air balance, 800 °C, 12 h	0.035 vol% NO, 0.035 vol% NH ₃ , 14 vol% O ₂ , 2.5 vol% H ₂ O, N ₂ balance, GHSV 100,000 h ⁻¹	200–500 (not shown)	77
14	(0.98 wt%)Cu-SSZ-13 ($n(\text{Si})/n(\text{Al}) = 6$)			200–500 (<5 ppm N ₂ O), *200–500 (not shown)	



Table 1 (Contd.)

Pos.	Sample	Preparation method	Reaction conditions	Operation temperature for achieving > 80% NO _x conversion/ ^o C ((by-)product formation)	Ref.
15	(0.88 wt%)Cu-SSZ-13 ($\eta(\text{Si})/\eta(\text{Al}) = 16$)	Ion-exchange, calcination, 550 °C, 8 h, air; pre-treatment: 21 vol% O ₂ , N ₂ balance, 500 °C, 2 h	0.05 vol% NO, 0.05 vol% NH ₃ , 5 vol% O ₂ , 10 vol% H ₂ O, N ₂ balance, GHSV 100,000 h ⁻¹	200–600 (not shown)	78
16	(0.95–1.38 wt%)Cu-SSZ-13 ($\eta(\text{Si})/\eta(\text{Al}) = 20$)	Ion-exchange; pre-treatment: 5 vol% O ₂ , He balance, 550 °C, 1 h	0.1 vol% NO, 0.1 vol% NH ₃ , 5 vol% O ₂ , He balance, GHSV 100,000 h ⁻¹	300–450 (not shown)	79
17	(1.04 wt%)Cu-SSZ-13 ($\eta(\text{Si})/\eta(\text{Al}) = 5.5$)	Ion-exchange, calcination, 500 °C, 5 h, air; *hydrothermal treatment: 10 vol% H ₂ O, air balance, 800 °C, 12 h	0.05 vol% NO, 0.05 vol% NH ₃ , 10 vol% O ₂ , 5 vol% H ₂ O, N ₂ balance, GHSV 30,000 h ⁻¹	200–600 (not shown), *200–550 (not shown)	80
18	(1.00–1.17 wt%)Cu-SSZ-13 ($\eta(\text{Si})/\eta(\text{Al}) = 23.6\text{--}23.8$)	Ion-exchange, calcination, 550 °C, 6 h, air; pre-treatment: 500 °C, 0.5 h, 5 vol% O ₂ , N ₂ balance	0.05 vol% NO, 0.05 vol% NH ₃ , 10 vol% O ₂ , 3 vol% H ₂ O, N ₂ balance, GHSV 40,000 h ⁻¹	250–500 (<6 ppm N ₂ O)	81
19	(2.5 wt%)Cu-SSZ-13 ($\eta(\text{Si})/\eta(\text{Al}) = 15$)	Ion-exchange, calcination, 500 °C, 5 h, air; *hydrothermal treatment: 10 vol% H ₂ O, air balance, 800 °C, 5 h	0.05 vol% NO, 0.05 vol% NH ₃ , 10 vol% O ₂ , 5 vol% H ₂ O, N ₂ balance, GHSV 80,000 h ⁻¹	175–550 (<15 ppm N ₂ O), *175–600 (<15 ppm N ₂ O)	82
20	(1.21 wt%)Cu-SSZ-13 ($\eta(\text{Si})/\eta(\text{Al}) = 6$)	Ion-exchange, calcination, 550 °C, 4 h, air; *hydrothermal treatment: 10 vol% H ₂ O, air balance, 600 °C, 20 h	0.036 vol% NO, 0.036 vol% NH ₃ , 10 vol% O ₂ , N ₂ balance, GHSV 400,000 h ⁻¹	225–550 (not shown), *250–550 (not shown)	83
21	(1.25–1.27 wt%)Cu-SSZ-13 ($\eta(\text{Si})/\eta(\text{Al}) = 21\text{--}24$)	Ion-exchange, calcination, 550 °C, 6 h, air; pre-treatment: 500 °C, 1 h, 14 vol% O ₂ , N ₂ balance; *hydrothermal treatment: 5 vol% H ₂ O, N ₂ balance, 800 °C, 16 h	0.005 vol% NO, 0.005 vol% NH ₃ , 5 vol% O ₂ , N ₂ balance, GHSV 48,000 h ⁻¹	200–500 (>90% N ₂ selectivity), *200–500 (>90% N ₂ selectivity)	84
22	(1.3 wt%)Cu-SSZ-13 ($\eta(\text{Si})/\eta(\text{Al}) = 17.6$)	Ion-exchange, calcination, 550 °C, 4 h, air; pre-treatment: 5 vol% O ₂ , He balance, 550 °C, 1 h	0.01 vol% NO, 0.01 vol% NH ₃ , 5 vol% O ₂ , He balance, GHSV 100,000 h ⁻¹	250–450 (not shown)	58
23	(1.45–1.62 wt%)Cu-SSZ-13 ($\eta(\text{Si})/\eta(\text{Al})$ not shown)	Ion-exchange, calcination, 550 °C, 5 h, air; *hydrothermal treatment: 10 vol% H ₂ O, air balance, 800 °C, 16 h	0.035 vol% NO, 0.035 vol% NH ₃ , 14 vol% O ₂ , 2.5 vol% H ₂ O, N ₂ balance, GHSV 200,000 h ⁻¹	200–500 (not shown), *225–450 (not shown)	14
24	(1.73 wt%)Cu-SSZ-13 ($\eta(\text{Si})/\eta(\text{Al}) = 9.5$)	Ion-exchange, calcination, 550 °C, 4 h, air; *hydrothermal treatment: 10 vol% H ₂ O, air balance, 800 °C, 16 h	0.05 vol% NO, 0.05 vol% NH ₃ , 5 vol% O ₂ , 5 vol% H ₂ O, N ₂ balance, GHSV 400,000 h ⁻¹	225–600 (>95% N ₂ selectivity), *250–500 (>90% N ₂ selectivity)	85
25	(1.8–2 wt%)Cu-SSZ-13 ($\eta(\text{Si})/\eta(\text{Al}) = 7.8$)	Ion-exchange, calcination, temperature and time not shown; *hydrothermal treatment: 5 vol% H ₂ O, N ₂ balance, 750 °C, 16 h	0.05 vol% NO, 0.05 vol% NH ₃ , 14 vol% O ₂ , 5 vol% H ₂ O, N ₂ balance, GHSV 48,000 h ⁻¹	200–600 (>97% N ₂ selectivity), *200–500 (>97% N ₂ selectivity)	86
26	(1.88–2.16 wt%)Cu-SSZ-13 ($\eta(\text{Si})/\eta(\text{Al}) = 16.5\text{--}20.3$)	Ion-exchange, calcination, 550 °C, 5 h, air; *hydrothermal treatment: 10 vol% H ₂ O, air balance, 750 °C, 16 h; pre-treatment: 21 vol% O ₂ , N ₂ balance, 550 °C, 20 min	0.05 vol% NO, 0.05 vol% NH ₃ , 5 vol% O ₂ , 3 vol% H ₂ O, N ₂ balance, GHSV 120,000 h ⁻¹	200–550 (<5 ppm N ₂ O), *200–500 (<5 ppm N ₂ O)	87
27	(2 wt%)Cu-SSZ-13 ($\eta(\text{Si})/\eta(\text{Al}) = 9$)	Ion-exchange, calcination, 550 °C, 5 h, air; *hydrothermal treatment: 10 vol% H ₂ O, air balance, 800 °C, 16 h; **degreening: 10 vol% H ₂ O, air balance, 700 °C, 4 h	0.036 vol% NO, 0.036 vol% NH ₃ , 14 vol% O ₂ , 2.5 vol% H ₂ O, N ₂ balance, GHSV 100,000 h ⁻¹	*200–550 (not shown), **200–550 (not shown)	88

Table 1 (Contd.)

Pos.	Sample	Preparation method	Reaction conditions	Operation temperature for achieving > 80% NO _x conversion/ ^o C ((by-)product formation)	Ref.
28	(2 wt%)Cu-SSZ-13 ($n(\text{Si})/n(\text{Al}) = 11$)	Ion-exchange, calcination conditions not shown; degreening: Reaction conditions, 600 °C, 4 h; pre-treatment: 10 vol% O ₂ , 7 vol% H ₂ O, N ₂ balance, 600 °C, 1 h	0.035 vol% NO, 0.035 vol% NH ₃ , 10 vol% O ₂ , 7 vol% H ₂ O, N ₂ balance, GHSV 300,000 h ⁻¹	225–550 (>97% N ₂ selectivity)	89
29	(2.08 wt%)Cu-SSZ-13 ($n(\text{Si})/n(\text{Al}) = 4.5$)	Ion-exchange, calcination, 550 °C, 4 h, air; hydrothermal treatment: 20 vol% O ₂ , 10 vol% H ₂ O, N ₂ balance, 550 °C, 0.5 h	0.05 vol% NO, 0.05 vol% NH ₃ , 10 vol% O ₂ , N ₂ balance, *0.05 vol% NO, 0.05 vol% NH ₃ , 10 vol% O ₂ , 5 vol% H ₂ O, N ₂ balance, GHSV 240,000 ml g ⁻¹ h ⁻¹	250–300 (not shown), *250–300 (not shown)	90
30	(2.1 wt%)Cu-SSZ-13 ($n(\text{Si})/n(\text{Al}) = 12$)	Ion-exchange, calcination conditions not shown; *hydrothermal treatment: 10 vol% H ₂ O, air balance, 800 °C, 16 h	0.036 vol% NO, 0.036 vol% NH ₃ , 14 vol% O ₂ , 2.5 vol% H ₂ O, N ₂ balance, GHSV 200,000 h ⁻¹	175–500 (not shown), *200–450 (not shown)	91
31	(2.2 wt%)Cu-SSZ-13 ($n(\text{Si})/n(\text{Al}) = 10.5$)	Ion-exchange, calcination, 600 °C, 6 h, air; *hydrothermal treatment: 10 vol% H ₂ O, air balance, 800 °C, 16 h	0.05 vol% NO, 0.05 vol% NH ₃ , 5 vol% O ₂ , 5 vol% H ₂ O, N ₂ balance, GHSV 400,000 h ⁻¹	225–550 (<10 ppm N ₂ O), *225–500 (<15 ppm N ₂ O)	92
32	(2.23 wt%)Cu-SSZ-13 ($n(\text{Si})/n(\text{Al}) = 8.8$)	Ion-exchange, calcination condition not shown; hydrothermal treatment: *700 °C (**800 °C), 10 vol% H ₂ O, air balance, 15 h	0.03 vol% NO, 0.03 vol% NH ₃ , 5 vol% O ₂ , 3 vol% H ₂ O, N ₂ balance, WHSV 60,000 ml g ⁻¹ h ⁻¹	250–500 (not shown), *250–500 (not shown), **300–350 (not shown)	93
33	(2.25 wt%)Cu-SSZ-13 ($n(\text{Si})/n(\text{Al}) = 12$)	Ion-exchange, calcination, 550 °C, 5 h, air; *hydrothermal treatment: 10 vol% H ₂ O, 700 °C, 16 h; pre-treatment: 14 vol% N ₂ balance, 500 °C, 1 h	0.036 vol% NO, 0.036 vol% NH ₃ , 14 vol% O ₂ , 2.5 vol% H ₂ O, N ₂ balance, GHSV 200,000 h ⁻¹	175–500 (<7 ppm N ₂ O), *200–500 (<25 ppm N ₂ O)	94
34	(2.3 wt%)Cu-SSZ-13 ($n(\text{Si})/n(\text{Al}) = 15$) monolith catalyst	Ion-exchange, calcination, 600 °C, 5 h, air; *hydrothermal treatment: 10 vol% H ₂ O, air balance, 750 °C, 12 h	0.1 vol% NO, 0.11 vol% NH ₃ , 5 vol% O ₂ , 10 vol% H ₂ O, N ₂ balance, GHSV 30,000 h ⁻¹	200–575 (not shown), *200–575 (not shown)	95
35	(2.35 wt%)Cu-SSZ-13 ($n(\text{Si})/n(\text{Al}) = 12.93$)	Ion-exchange, calcination, 550 °C, 4 h, air; pre-treatment: 8 vol% O ₂ , N ₂ balance, 1 h, 500 °C	0.05 vol% NO, 0.05 vol% NH ₃ , 6.5 vol% O ₂ , 3 vol% H ₂ O, N ₂ balance, GHSV 120,000 h ⁻¹	125–400 (>95% N ₂ selectivity)	96
36	(2.38 wt%)Cu-SSZ-13 ($n(\text{Si})/n(\text{Al}) = 6$)	Ion-exchange, calcination, 600 °C, time not shown, air; pre-treatment: 5 vol% O ₂ , N ₂ balance, 200 °C, 1 h	0.06 vol% NO, 0.06 vol% NH ₃ , 5 vol% O ₂ , 5 vol% H ₂ O, N ₂ balance, GHSV 450,000 h ⁻¹	250–550 (not shown)	97
37	(2.38 wt%)Cu-SSZ-13 ($n(\text{Si})/n(\text{Al}) = 6$)	Ion-exchange, calcination, 600 °C, 6 h, air; *hydrothermal treatment: 10 vol% H ₂ O, air balance, 750 °C, 16 h; pre-treatment: 5 vol% O ₂ , N ₂ balance, 1 h, 600 °C	0.05 vol% NO, 0.05 vol% NH ₃ , 5 vol% O ₂ , 5 vol% H ₂ O, N ₂ balance, GHSV not shown	250–550 (not shown), *300–400 (not shown)	98
38	(2.5–3 wt%)Cu-SSZ-13 ($n(\text{Si})/n(\text{Al}) = 12.5$)	Ion-exchange, calcination, 500 °C, 6 h, air; *hydrothermal treatment: 5 vol% H ₂ O, air balance, 800 °C, 12 h	0.1 vol% NO, 0.1 vol% NH ₃ , 5 vol% O ₂ , N ₂ balance, GHSV 130,000 h ⁻¹	200–800 (100% N ₂ selectivity), *200–800 (100% N ₂ selectivity)	30
39	(2.5 wt%)Cu-SSZ-13 ($n(\text{Si})/n(\text{Al}) = 8.7$)	Ion-exchange, calcination, 550 °C, 5 h, air; *hydrothermal treatment: 10 vol% H ₂ O, air balance, 750 °C, 16 h	0.05 vol% NO, 0.05 vol% NH ₃ , 5 vol% O ₂ , 5 vol% H ₂ O, N ₂ balance, GHSV 200,000 h ⁻¹	200–550 (100% N ₂ selectivity), *250–500 (100% N ₂ selectivity)	99
40	(2.5 wt%)Cu-SSZ-13 ($n(\text{Si})/n(\text{Al})$ not shown)	Ion-exchange, calcination, 550 °C, 6 h, air; *one-pot hydrothermal synthesis, calcination, 550 °C, 6 h, air	0.05 vol% NO, 0.05 vol% NH ₃ , 5 vol% O ₂ , Ar balance, GHSV 180,000 h ⁻¹	250–600 (not shown), *200–600 (not shown)	100





Table 1 (Contd.)

Pos.	Sample	Preparation method	Reaction conditions	Operation temperature for achieving > 80% NO _x conversion/ ^o C ((by-)product formation)	Ref.
41	(2.8 wt%)Cu-SSZ-13 ($n(\text{Si})/n(\text{Al}) = 5$)	Ion-exchange, calcination, 550 °C, 5 h, air; *hydrothermal treatment: 10 vol% H ₂ O, air balance, 800 °C, 16 h	0.05 vol% NO, 0.05 vol% NH ₃ , 10 vol% O ₂ , 5 vol% H ₂ O, N ₂ balance, GHSV 80,000 h ⁻¹	175–650 (<15 ppm N ₂ O), *175–550 (<15 ppm N ₂ O)	101
42	(3.0 wt%)Cu-SSZ-13 ($n(\text{Si})/n(\text{Al}) = 6$)	Ion-exchange, calcination, 550 °C, 8 h, air; *hydrothermal treatment: 10 vol% H ₂ O, air balance, 800 °C, 16 h	0.036 vol% NO, 0.036 vol% NH ₃ , 14 vol% O ₂ , 2.5 vol% H ₂ O, N ₂ balance, GHSV 100,000 h ⁻¹	200–450 (not shown)	102
43	(3.4 wt%)Cu-SSZ-13 ($n(\text{Si})/n(\text{Al}) = 9$)	Ion-exchange, calcination, 700 °C, 5 h, air	0.05 vol% NO, 0.05 vol% NH ₃ , 4 vol% O ₂ , N ₂ balance, GHSV 60,000 h ⁻¹	175–500 (<10 ppm N ₂ O)	103
44	(3.43–5.15 wt%)Cu-SSZ-13 ($n(\text{Si})/n(\text{Al}) = 6$)	Ion-exchange, calcination, 550 °C, 8 h, air	0.035 vol% NO, 0.035 vol% NH ₃ , 14 vol% O ₂ , 2.5 vol% H ₂ O, N ₂ balance, GHSV 80,000 h ⁻¹	250–550 (not shown)	32
45	(3.6 wt%)Cu-SSZ-13 ($n(\text{Si})/n(\text{Al}) = 6.5$) monolith catalyst	Ion-exchange, calcination, 700 °C, 4 h, air	0.02 vol% NO, 0.02 vol% NH ₃ , 8 vol% O ₂ , 10 vol% H ₂ O, N ₂ balance, GHSV 60,000 h ⁻¹	200–500 (>95% N ₂ selectivity)	104
46	(3.97 wt%)Cu-SSZ-13 ($n(\text{Si})/n(\text{Al}) = 13.26$)	Ion-exchange, calcination, 550 °C, 6 h, air	0.05 vol% NO, 0.05 vol% NH ₃ , 10 vol% O ₂ , 5 vol% H ₂ O, N ₂ balance, GHSV 100,000 h ⁻¹	200–450 (>95% N ₂ selectivity)	64
47	(4.0–4.7 wt%)Cu-SSZ-13 ($n(\text{Si})/n(\text{Al}) = 12.0–12.7$)	Ion-exchange, calcination, 500 °C, 6 h, air; *hydrothermal treatment: 10 vol% H ₂ O, air balance, 800 °C, 12 h	0.05 vol% NO, 0.05 vol% NH ₃ , 10 vol% O ₂ , N ₂ balance, GHSV 30,000 h ⁻¹	200–500 (<25 ppm N ₂ O), *200–500 (<25 ppm N ₂ O)	48
48	(4.1 wt%)Cu-SSZ-13 ($n(\text{Si})/n(\text{Al}) = 6$) monolith catalyst	Ion-exchange, calcination, 600 °C, 4 h, air	0.04 vol% NO, 0.04 vol% NH ₃ , 8 vol% O ₂ , 5 vol% H ₂ O, Ar balance, GHSV 22,100 h ⁻¹	175–500 (<15 ppm NO ₂ , <8 ppm N ₂ O)	105
49	(4.93 wt%)Cu-SSZ-13 ($n(\text{Si})/n(\text{Al}) = 6.48$)	Ion-exchange, calcination, 550 °C, 6 h, air	0.1 vol% NO, 0.1 vol% NH ₃ , 6 vol% O ₂ , 5 vol% H ₂ O, He balance, GHSV 50,000 h ⁻¹	150–450 (>70% N ₂ yield)	16
50	(4.93 wt%)Cu-SSZ-13 ($n(\text{Si})/n(\text{Al}) = 4.03$)	Ion-exchange, vacuum evaporator, calcination, 550 °C, 6 h, air	0.1 vol% NO, 0.1 vol% NH ₃ , 10 vol% O ₂ , He balance, GHSV 30,000 h ⁻¹	150–450 (>70% N ₂ yield)	17
One-pot hydrothermal synthesis					
51	Cu-SSZ-13 ($n(\text{Si})/n(\text{Al}) = 14.2$) (Cu content not shown)	One-pot hydrothermal synthesis, calcination, 550 °C, time not shown, air; *hydrothermal treatment: 2.2 ml min ⁻¹ H ₂ O, air balance, 750 °C, 13 h pre-treatment: 550 °C, 1 h, N ₂	0.05 vol% NO, 0.053 vol% NH ₃ , 7 vol% O ₂ , 5 vol% H ₂ O, N ₂ balance, WHSV 450,000 ml g ⁻¹ h ⁻¹	250–500 (not shown), *300–450 (not shown)	62
52	(2.82 wt%)Cu-SSZ-13 ($n(\text{Si})/n(\text{Al}) = 15$) monolith catalyst	One-pot hydrothermal synthesis, calcination, 600 °C, 5 h, air; *hydrothermal treatment: 10 vol% H ₂ O, air balance, 850 °C, 12 h	0.1 vol% NO, 0.11 vol% NH ₃ , 5 vol% O ₂ , 10 vol% H ₂ O, N ₂ balance, GHSV 30,000 h ⁻¹	200–550 (not shown), *250–550 (not shown)	63
53	(3.5 wt%)Cu-SSZ-13 ($n(\text{Si})/n(\text{Al}) = 6.5$)	One-pot hydrothermal synthesis, calcination, 600 °C, 6 h, air; *hydrothermal treatment: 10 vol% H ₂ O, air balance, 750 °C, 16 h	0.05 vol% NO, 0.05 vol% NH ₃ , 5 vol% O ₂ , N ₂ balance, GHSV 400,000 h ⁻¹	200–600 (>90% N ₂ selectivity), *200–550 (>90% N ₂ selectivity)	106

Table 1 (Contd.)

Pos.	Sample	Preparation method	Reaction conditions	Operation temperature for achieving > 80% NO _x conversion/ ^o C ((by-)product formation)	Ref.
54	(3.8 wt%)Cu-SSZ-13 ($n(\text{Si})/n(\text{Al}) = 8.3$)	One-pot hydrothermal synthesis, calcination, 600 °C, 6 h, air; *hydrothermal treatment: 10 vol% H ₂ O, air balance, 750 °C, 16 h	0.05 vol% NO, 0.05 vol% NH ₃ , 5 vol% O ₂ , N ₂ balance, GHSV 400,000 h ⁻¹	200–550 (100% N ₂ selectivity), *250–450 (not shown)	67
55	(4.06–4.11 wt%)Cu-SSZ-13 ($n(\text{Si})/n(\text{Al}) = 4$)	One-pot hydrothermal synthesis, calcination, 600 °C, 6 h, air; *hydrothermal treatment: 10 vol% H ₂ O, air balance, 750 °C, 12 h; pre-treatment: 5 vol% O ₂ , N ₂ balance, 550 °C, 1 h	0.05 vol% NO, 0.05 vol% NH ₃ , 5 vol% O ₂ , 5 vol% H ₂ O, N ₂ balance, WHSV 300,000 ml g ⁻¹ h ⁻¹	175–550 (<10 ppm N ₂ O), *175–450 (<20 ppm N ₂ O)	107
56	(4.92 wt%)Cu-SSZ-13 ($n(\text{Si})/n(\text{Al}) = 4.36$)	One-pot hydrothermal synthesis, calcination, 550 °C, 4 h, air; *hydrothermal treatment: 10 vol% H ₂ O, air balance, 750 °C, 16 h; pre-treatment: Reaction conditions, 550 °C, 1 h	0.05 vol% NO, 0.05 vol% NH ₃ , 5 vol% O ₂ , 5 vol% H ₂ O, N ₂ balance, GHSV 300,000 h ⁻¹	200–500 (not shown), *250–500 (not shown)	108
57	(6.31 wt%)Cu-SSZ-13 ($n(\text{Si})/n(\text{Al}) = 13$)	One-pot hydrothermal synthesis, calcination, 600 °C, 6 h, air	0.05 vol% NO, 0.05 vol% NH ₃ , 5 vol% O ₂ , N ₂ balance, GHSV 100,000 h ⁻¹	150–550 (not shown)	65
58	(9.5 wt%)Cu-SSZ-13 ($n(\text{Si})/n(\text{Al}) = 4$)	One-pot hydrothermal synthesis, calcination, 550 °C, 8 h, air	0.1 vol% NO, 0.1 vol% NH ₃ , 10 vol% O ₂ , Ar balance, GHSV not shown	150–450 (not shown)	61
59	(9.7 wt%)Cu-SSZ-13 ($n(\text{Si})/n(\text{Al}) = 3.82$)	One-pot hydrothermal synthesis, calcination, 550 °C, 6 h, air	0.06 vol% NO, 0.06 vol% NH ₃ , 6 vol% O ₂ , 5 vol% H ₂ O, He balance, GHSV 400,000 h ⁻¹	200–550 (>98% N ₂ selectivity)	109
60	(10.0 wt%)Cu-SSZ-13 ($n(\text{Si})/n(\text{Al}) = 4.5$)	One-pot hydrothermal synthesis, calcination, 600 °C, 6 h, air	0.05 vol% NO, 0.05 vol% NH ₃ , 5 vol% O ₂ , 5 vol% H ₂ O, N ₂ balance, GHSV 400,000 h ⁻¹	225–400 (not shown)	110
61	(10.61 wt%)Cu-SSZ-13 ($n(\text{Si})/n(\text{Al}) = 4.17$)	One-pot hydrothermal synthesis, calcination, 550 °C, 6 h, air	0.05 vol% NO, 0.05 vol% NH ₃ , 5 vol% O ₂ , N ₂ balance, GHSV 120,000 h ⁻¹	150–400 (>90% N ₂ selectivity)	111
62	(11.27 wt%)Cu-SSZ-13 ($n(\text{Si})/n(\text{Al}) = 4.2$)	One-pot hydrothermal synthesis, calcination, 600 °C, 5 h, air	500 ml m ⁻³ NO, 500 ml m ⁻³ NH ₃ , 10 vol% O ₂ , N ₂ balance, GHSV 180,000 h ⁻¹	200–400 (>95% N ₂ selectivity)	66
Solid-state ion-exchange					
63	(1.79 wt%)Cu-SSZ-13 ($n(\text{Si})/n(\text{Al}) = 10.8$)	Solid-state ion-exchange, vacuum evaporator, calcination, 300 °C, 0.5 h, air; *hydrothermal treatment: 10 vol% H ₂ O, air balance, 750 °C, 16 h	0.05 vol% NO, 0.05 vol% NH ₃ , 5 vol% O ₂ , 3 vol% H ₂ O, N ₂ balance, GHSV 120,000 h ⁻¹	200–550 (not shown), *200–550 (not shown)	112
64	(3.7 wt%)Cu-SSZ-13 ($n(\text{Si})/n(\text{Al}) = 13$)	Solid-state ion-exchange, calcination, 600 °C, 5 h, 800 °C 12 h, air	0.04 vol% NO, 0.04 vol% NH ₃ , 8 vol% O ₂ , 5 vol% H ₂ O, Ar balance, GHSV 205,000 h ⁻¹	250–500 (not shown)	113
65	(3.08 wt%)Cu-SSZ-13 ($n(\text{Si})/n(\text{Al}) = 10.1$) monolith catalyst	Solid-state ion-exchange, vacuum evaporator, calcination conditions not shown; *hydrothermal treatment: 10 vol% H ₂ O, air balance, 800 °C, 12 h	0.1 vol% NO, 0.11 vol% NH ₃ , 10 vol% O ₂ , N ₂ balance, GHSV 80,000 h ⁻¹	200–550 (>90% N ₂ selectivity), *200–550 (not shown)	47





Table 1 (Contd.)

Pos.	Sample	Preparation method	Reaction conditions	Operation temperature for achieving > 80% NO _x conversion/ ^o C ((by-)product formation)	Ref.
66	(3.9 wt%)Cu-SSZ-13 ($r(\text{Si})/r(\text{Al}) = 5.2$)	Solid-state ion-exchange, calcination, 600 °C, time not shown, air; *hydrothermal treatment: 10 vol% H ₂ O, air balance, 750 °C, 16 h	0.05 vol% NO, 0.05 vol% NH ₃ , 5 vol% O ₂ , 5 vol% H ₂ O, N ₂ balance, GHSV 400,000 h ⁻¹	200–550 (>97% N ₂ selectivity), *200–450 (not shown)	114
67	(4.10 wt%)Cu-SSZ-13 ($r(\text{Si})/r(\text{Al}) = 6$)	Solid-state ion-exchange, calcination, 700 °C, 16 h, dry air; *hydrothermal treatment: 10 vol% H ₂ O, 10 vol% O ₂ , N ₂ balance, 750 °C, 16 h	0.05 vol% NO, 0.05 vol% NH ₃ , 10 vol% O ₂ , 10 vol% H ₂ O, N ₂ balance, GHSV 240,000 h ⁻¹	225–550 (not shown), *225–500 (not shown)	115
Impregnation					
68	(1.5 wt%)Cu-SSZ-13 ($r(\text{Si})/r(\text{Al}) = 12.6$)	Impregnation, calcination, 550 °C, 1 h, air	0.02 vol% NO, 0.02 vol% NH ₃ , 10 vol% O ₂ , 3 vol% H ₂ O, N ₂ balance, GHSV 60,000 h ⁻¹	200–500 (not shown)	69
69	(1.5 wt%)Cu-SSZ-13 ($r(\text{Si})/r(\text{Al}) = 11.5$)	Impregnation, calcination, 550 °C, 1 h, air; *hydrothermal treatment: 10 vol% H ₂ O, air balance, 900 °C, 4 h, **8 h	0.02 vol% NO, 0.02 vol% NH ₃ , 10 vol% O ₂ , 3 vol% H ₂ O, N ₂ balance, GHSV 60,000 h ⁻¹	200–500 (not shown), *200–500 (not shown), **200–500 (not shown)	116
70	(2 wt%)Cu-SSZ-13 ($r(\text{Si})/r(\text{Al}) = 11.4$) monolith catalyst	Impregnation, calcination, 600 °C, 8 h; 750 °C, 2 h, air; degreening: 0.04 vol% NO, 0.04 vol% NH ₃ , 5 vol% H ₂ O, Ar balance, 250 °C, 1 h; 10 vol% O ₂ , 500 °C; pre-treatment: 10 vol% O ₂ , 5 vol% H ₂ O, Ar balance, 500 °C, 20 min	0.04 vol% NO, 0.04 vol% NH ₃ , 10 vol% O ₂ , Ar balance, *0.04 vol% NO, 0.04 vol% NH ₃ , 10 vol% O ₂ , 5 vol% H ₂ O, Ar balance, GHSV 20,400 h ⁻¹	250–500 (>3 ppm N ₂ O), *200–500 (<5 ppm N ₂ O)	117
71	(2.2 wt%)Cu-SSZ-13 ($r(\text{Si})/r(\text{Al}) = 12$)	Impregnation, 550 °C, 5 h, air; degreening: 10 vol% H ₂ O, air balance, 650 °C, 4 h; *hydrothermal treatment: 10 vol% H ₂ O, air balance, 800 °C, 16 h	0.036 vol% NO, 0.036 vol% NH ₃ , 14 vol% O ₂ , 2.5 vol% H ₂ O, N ₂ balance, GHSV 100,000 h ⁻¹	175–500 (not shown), *175–400 (not shown)	118

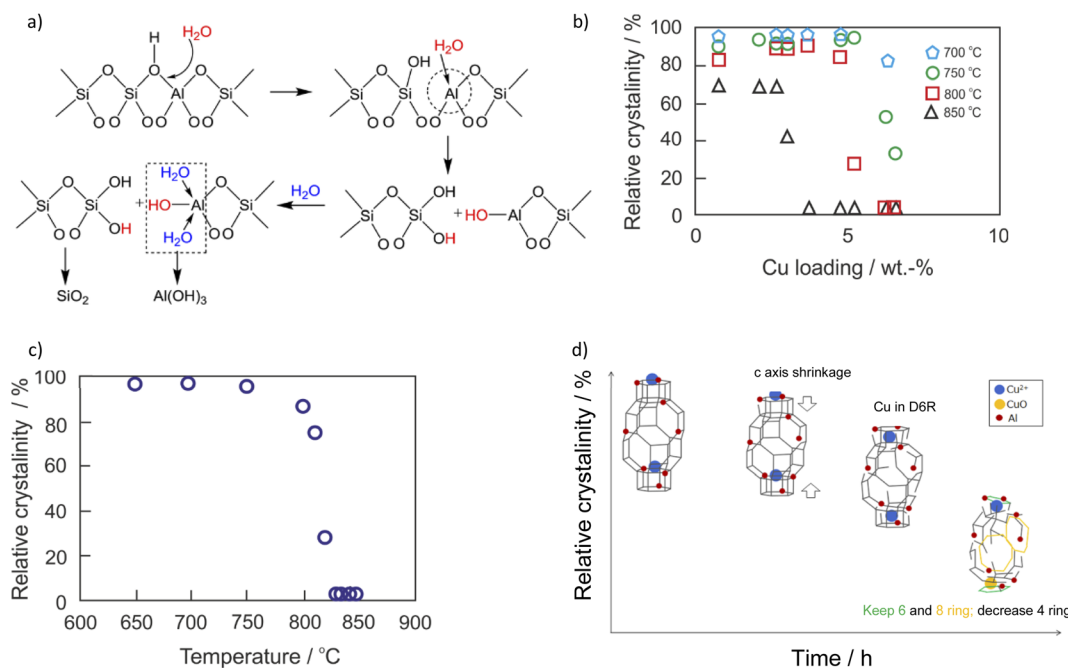


Fig. 3 (a) Zeolite hydrolysis process. Reproduced from ref. 77 with permission from ACS Publications, copyright 2015; (b) effect of copper loading on the hydrothermal stability of Cu-SSZ-13. The hydrothermal stability test was conducted at several temperatures for 5 h in flowing air containing 10 vol% H₂O. The crystallinity of the solid product was calculated based on the areas on the peaks in the 2θ range from 20° to 32° in its XRD pattern, and Cu-SSZ-13 before hydrothermal aging was chosen as the standard for the crystallinity calculation. Reproduced from ref. 104 with permission from ACS Publications, copyright 2018; (c) (3.6 wt%)Cu-SSZ-13 ($n(\text{Si})/n(\text{Al}) = 6.5$) degradation curve by XRD. The hydrothermal stability test was conducted at several temperatures for 5 h in flowing air containing 10 vol% H₂O; (d) proposed degradation scheme for Cu-SSZ-13. Reproduced from ref. 126 with permission from ACS Publications, copyright 2019.

One-pot hydrothermal method

Cu-containing SSZ-13 prepared by the one-pot hydrothermal method shows higher content and dispersion of copper species.⁶⁰ Ren *et al.*⁶¹ designed a one-pot synthesis method for Cu-SSZ-13 (with a low $n(\text{Si})/n(\text{Al})$ ratio of 4) using low-cost copper-tetraethylenepentamine (Cu-TEPA) as a template. The catalyst exhibited superior catalytic activity with more than 80% NO conversion at 150–450 °C. In addition, Martínez-Franco *et al.*⁶² used Cu-TEPA and *N,N,N*-trimethyl-1-adamantonium (TMAdaOH) in one-pot prepared Cu-SSZ-13 with $n(\text{Si})/n(\text{Al})$ of 14.2 and Cu loading of $n(\text{Cu})/n(\text{Si} + \text{Al}) = 0.059$, *i.e.*, controlled ratios and a Cu loading. Furthermore, in another study,⁶³ a $n(\text{Si})/n(\text{Al})$ ratio of 15 was reported to guarantee enhanced NO conversion among $n(\text{Si})/n(\text{Al})$ ratios of 6, 15 and 30. In other studies, the authors mentioned $n(\text{Si})/n(\text{Al})$ of 13.26 (among 6.54–33.12)⁶⁴ or 13 (among 10.6, 13.0 and 16.0)⁶⁵ for Cu-SSZ-13 prepared *via* the one-pot hydrothermal method, and investigated its activity for the NH₃-SCR-DeNO_x.

One of the main drawbacks of the one-pot hydrothermal method appears to be a high loading of copper species (*i.e.*, 6.31–11.27 wt% of Cu) as the result of a large amount of metal ions in the corresponding structure-directing agent^{61,65,66} (Table 1, pos. 57–62). Unfortunately, these copper ions cannot be completely removed, even after an ion-exchange (*i.e.*, reverse ion-exchange) of Cu-SSZ-13 with an aqueous solution of 1 M NH₄NO₃ for several times,⁶⁷ limiting its control. Following these studies, the synthesis was further optimized by decreasing the amount of

template required and changing some post-treatment steps (*e.g.*, with dilute HNO₃ solution or with HNO₃ followed by NH₄NO₃ solution)^{60,66,67,110,114,119} or even *via* the introduction of a second transition metal.¹¹¹ As a result, materials with a significantly lower amount of copper species (*e.g.*, <3.9 wt%) were achieved, thus, enhancing its activity in NH₃-SCR-DeNO_x (Fig. 2c). For example, Liu *et al.*⁶⁶ reported an effective strategy to regulate the nature and distribution of Cu species of a one-pot synthesized Cu-SSZ-13 zeolite *via* ion-exchange with an aqueous 0.1 M HNO₃ solution (for 4, 8, 12 and 16 h) before removing the template. An optimum time of 4 h guarantees enlarged specific surface area, pore volume, $n(\text{Si})/n(\text{Al})$ ratio and isolated Cu²⁺ content, and thus enhanced activity and N₂ selectivity over Cu-SSZ-13.

Solid-state ion-exchange

Relatively limited studies – compared to Cu-SAPO-34,¹²⁰ were conducted on Cu-containing SSZ-13 prepared *via* solid-state ion-exchange (SSIE, Table 1, pos. 63–67). However, it has been reported that SSIE can be carried out either *via* the physical mixture of CuO and H-SSZ-13 at 700–800 °C (reduction of Cu²⁺ in CuO to Cu⁺/Cu⁰, and reoxidation at the ion-exchange sites of the zeolites)^{47,115} or ammonia-assisted SSIE (below 350 °C, formation of the [Cu(NH₃)₂]⁺ complex *via* the interaction of Cu₂O(111) with H- or NH₄⁺-SSZ-13).¹²¹ In the first approach, framework deteriorations and inadequately reacted CuO_x was inevitable, while in the second approach the application of ammonia may limit the commercialization of the NH₃-assisted



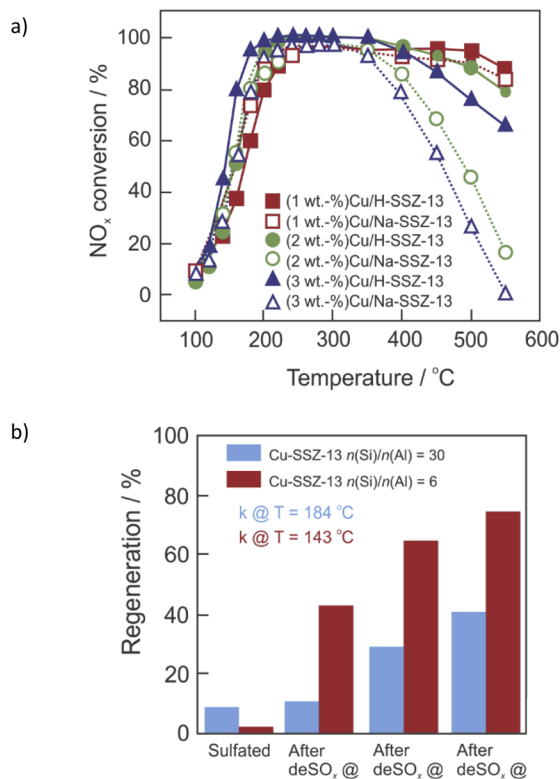


Fig. 4 (a) NO_x conversion over degreened Cu-H-SSZ-13 and Cu-Na-SSZ-13. Reproduced from ref. 88 with permission from Elsevier, copyright 2020; (b) NH₃-SCR-DeNO_x activity regeneration after stepwise desulfation at different temperatures based on rate constant measured at *T* = 143 °C for Cu-SSZ-13 (*n*(Si)/*n*(Al) = 6), and *T* = 184 °C for Cu-SSZ-13 (*n*(Si)/*n*(Al) = 30). Reproduced from ref. 137 with permission from ACS Publications, copyright 2018.

SSIE. Moreover, the modification of HT-SSIE (e.g., after 150–500 °C NH₃-SCR-DeNO_x due to movement of external CuO to Cu²⁺ ions inside the zeolite channels under reaction conditions¹¹³), or LT-SSIE (e.g., application of the copper salts that decompose below 300 °C),¹²² as well as the use of NO and NH₃ for the generation of the [Cu(NH₃)_x]⁺ (≥2),¹¹² were reported. Furthermore, Zhang *et al.*⁴⁷ claimed that the application of the NH₄⁺-form (rather than the H-form) led to the presence of more Cu²⁺ ions and fewer CuO_x species. The formation of [Cu(NH₃)_x]²⁺ intermediates (*x* = 2 or 4) promotes the mobility of Cu²⁺ species, facilitating its introduction into ion-exchange sites, which was favorable for NH₃-SCR-DeNO_x (Fig. 2d).

Hydrothermal stability and poisoning

NH₃-SCR-DeNO_x catalysts used in diesel vehicles operate under high temperature and humid conditions alongside poisons derived from biodiesel and lubricant oil additives. The activity and stability of respective Cu-containing SSZ-13 vary in NH₃-SCR-DeNO_x depending on the applied hydrothermal aging treatment (Table 1). Both the dealumination of the Cu-containing SSZ-13 catalysts, as well as the transformation of ZCuOH sites to Z₂Cu, coupled with the consumption of Brønsted acid sites, were reported during the rather mild hydrothermal aging treatment ≤

700 °C (ZCuOH + ZH → Z₂Cu + H₂O;^{69,75,83,91,123} confirmed *via* DFT calculations;⁸³ promoted by other transition metals^{44,99}). Water molecules tend to attack the aluminum sites (*i.e.*, Brønsted acid sites, –Si(OH)–Al–), which causes dealumination and consequently structural amorphization (decomposed to SiO₂ and Al(OH)₃, Fig. 3a).^{77,124,125} Al(OH)₃ possesses a kinetic diameter of 0.503 nm, which means that it cannot escape from the SSZ-13 pores during hydrothermal treatments. Thus, it can be inserted back into the framework during cooldown (*i.e.*, reversible dealumination) to maintain the integrity of the zeolite structure.¹⁹ The aluminum sites can be protected by adjusting the *n*(Si)/*n*(Al) ratio accordingly, thus accommodating the highly hydrothermally stable Cu²⁺-2Z sites. The Cu-SSZ-13 catalysts (*n*(Si)/*n*(Al) = 6–11, <3 wt%) are reported to be resistant to hydrothermal aging with 10 vol% H₂O at 800 °C for 16 h (*i.e.*, comparable to the exposure of a 135 000-mile vehicle-aged catalyst^{20,21,92}), which is influenced by the copper species loading (Fig. 3b).¹⁰⁴ A high copper loading is attributed to the abundance of [Cu(OH)]⁺-Z sites that tend to gradually transform to CuO_x upon hydrothermal aging, which further destabilizes the zeolite framework.^{33,80,91} However, the onset of zeolite-framework occurs above 800–900 °C^{21,126} (Fig. 3c). During the hydrothermal aging (>700 °C) of Cu-SSZ-13, [Cu(OH)]⁺-Z (rather than Cu²⁺-2Z) convert to CuO_x clusters *via* [Cu(OH)]⁺-Z → Cu(OH)₂ → CuO_x sequence, where [Cu(OH)]⁺-Z is first hydrolyzed to Cu(OH)₂, and then the latter agglomerates to form CuO_x clusters.^{91,127,128} Furthermore, CuO_x can interact with Al species without the formation of defined structures.¹²⁹ CuO_x clusters lower NH₃-SCR-DeNO_x selectivity by catalyzing the NH₃ oxidation side reactions, as well as actively promoting the degradation of SSZ-13 during aging. It was observed that hydrothermal aging at 800 °C for 16 h led to a significant increase in mesopores ≤ 4 nm, which is believed to result from increased CuO_x formation.^{80,91,127} The hydrothermal treatment causes the zeolite structure to contract in the *c* direction which then leads to the collapse of the 4MRs¹²⁶ (Fig. 3d). Despite this, some of the isolated copper species are still protected in the larger rings. Proding *et al.*¹⁴ reported higher hydrothermal stability over sub-micron Cu/SSZ-13 compared to Cu/SSZ-13 with particle sizes 10 times bigger.

Co-cation modification

The introduction of second metal ions into the Cu-containing SSZ-13 catalyst is a facile way to improve its hydrothermal stability. Sodium is a common element found in Cu-SSZ-13 as a result of a strong basic environment provided by NaOH during SSZ-13 synthesis and incomplete exchange between Na-SSZ-13 and NH₄NO₃ solutions (before Cu-exchange). For example, Gao *et al.*⁷⁷ demonstrated that the presence of certain amounts of Na⁺ (1.78 wt%) or Li⁺ (0.40 wt%) enhanced the hydrothermal stability of low-Cu loaded (0.87 wt%) Cu-SSZ-13 (*n*(Si)/*n*(Al) = 6). Further studies confirmed an optimal loading of 1–1.5 wt% of Na⁺ in the materials with preserved NO_x activity (Fig. 4a).⁸⁸ The optimized Al-rich (2.7 wt%)Cu–(1.7 wt%)Na-SSZ-13 (*n*(Si)/*n*(Al) = 4) catalyst exhibits >80% NO conversion between 200–650 °C in NH₃-SCR-DeNO_x after hydrothermal aging at 750 °C.⁸² The Na⁺ cations were reported to compete with Cu ions for catalytic



exchange sites and provide NH_3 adsorption function as Lewis acids, as well as neutralize Brønsted acid sites ($-\text{Si}(\text{OH})-\text{Al}-$; thus preventing dealumination during hydrothermal aging).^{77,88} The K^+ cations show effects similar to those of Na^+ and the optimal low-temperature activity for Cu, K-SSZ-13 is also found at $n(\text{K})/n(\text{Cu}) = 0.7$.¹⁰² Cu^{2+} ions occupy windows of 6MRs and co-cations occupy windows of 8MRs.¹⁰² Furthermore, the hydrothermal stability of (3.4–4.1 wt%)Cu-SSZ-13 was remarkably enhanced through loading with a small amount of cerium (*i.e.*, ca. 0.2–0.4 wt%, optimum ca. 0.35 wt%).¹⁰⁴ This can be achieved either *via* ion-exchange or solid-state ion-exchange. Cerium ions can serve as an oxygen reservoir that can store and release oxygen *via* the redox shift between Ce^{4+} and Ce^{3+} under oxidizing and reducing conditions, which presumably stabilize the zeolite framework. Also, Ce^{3+} ions tend to fill defect sites of zeolites, where they attract water molecules, reducing the probability of them attacking the aluminum sites. Other cations, like Ca^{2+} , are detrimental at any loading,¹⁰² according to the order of poisoning effect: $\text{Mg} > \text{Ca} > \text{Na} > \text{K}$.¹³⁰ The hydrothermal stability of Cu-SSZ-13 can be further improved *via* its modification with Fe,^{94,131} Y,¹⁰¹ Sm^{132,133} or Zn,¹⁰⁹ as well as by the passivation of its surface with Al_2O_3 ⁸⁷ or ZrO_2 .¹¹⁸ Furthermore, the hydrothermal stability of the composite samples, *e.g.*, Cu-SSZ-13 + Fe-SSZ-13,¹³⁴ H-SAPO-34, Cu-SSZ-13,⁹⁸ Cu-SSZ-13 and Cu-SAPO-34,^{135,136} was significantly improved compared to that of the single Cu-SSZ-13.

Sulfur poisoning

Thus, in addition to their excellent catalytic activity, hydrothermal stability and high resistance against chemical poisons are also highly required properties for these catalysts. As it also happens with hydrothermal stability, $[\text{Cu}(\text{OH})]^+-\text{Z}$ is more susceptible (than $\text{Cu}^{2+}-\text{Z}$) to SO_2 poisoning (coming from the burning of sulfurous species in fuel). Sulfur species adsorb on the ZCuOH sites (in the presence and absence of NH_3), and exist in bisulfate form ($\text{ZCuOH} + \text{SO}_2 \rightarrow \text{ZCuHSO}_3$). Moreover, ammonium sulfate ($(\text{NH}_4)_2\text{SO}_4$) blocks the Z_2Cu sites along with Cu sulfate species – CuHSO_4 (in the presence of NH_3 and SO_2) and Cu sulfate (in the presence of only SO_2 in the feed).¹³⁷ The lower mobility of sulfated Cu species compared to non-sulfated Cu species led to a drop in catalyst activity.⁶⁹ Ammonium sulfate can be removed at 350 °C,^{138,139} while in the case of other species temperatures higher than 550 °C were needed (*i.e.*, can be removed *via* regeneration of the diesel particle filter).^{137,140} Non-decomposed sulfate species block the pore of Cu-SSZ-13, thus decreasing its catalytic activity. However, many researchers showed that NO_x conversion can reach its original level after the removal of SO_2 and/or H_2O from the feed gas, *i.e.*, reversible inactivation.^{64,84} A combination of other metals (*e.g.*, Zn,¹⁴¹ Ce,^{142–144} Fe,^{43,145,146} *etc.*) with Cu-containing SSZ-13 can adequately protect active sites from sulfur poisoning. Furthermore, Cu-SSZ-13 becomes more robust against sulfur as a result of hydrothermal aging.⁶⁹

Phosphorus poisoning

Besides poisoning by sulfur-containing species, Cu-containing SSZ-13 is also affected by phosphorus and zinc (coming from

engine lubricating oil, *e.g.*, zinc dialkyldithiophosphate (ZDDP) as an additive), alkali and alkaline earth metals (*e.g.*, Na, K, Ca, and Mg, coming from engine lubricating oil), noble metals (coming from the upper stream emission abatement components, *e.g.*, diesel oxidation catalysts (DOC), *etc.*^{147–149}). Lezcano-Gonzalez *et al.*¹⁵⁰ gave an overview of the key deactivation mechanism observed for Ca, Zn, (1–2 wt%) Pt and P. Doping of Cu-SSZ-13 with P (2.2 wt%) fully suppressed the catalytic activity as a result of site blocking of the zeolite framework, CuO formation coupled with the reduction in the number of isolated Cu^{2+} ions, between other phenomena. In other studies, the catalyst's activity with higher P loading of 0.4–1.0 wt%, was significantly lower than that without P between 100 to 300 °C.⁹⁶ The N_2 selectivity was not affected by phosphorus at low temperatures. However, the introduction of Ca and Zn (1.3–5.4 and 2.2–8.8 wt%, respectively) led mainly to pore-blocking/filling together with the formation of CuO species. It has been widely reported that Pt species promote N_2O and NO_2 formation.^{107,150,151} Regarding the P-poisoning studies, Dahlin *et al.*⁵² investigated the activity of Cu-SSZ-13 exposed to exhaust generated by a biodiesel burner. Cu-SSZ-13 was deactivated at low temperatures, and could not be regenerated until temperatures up to 550 °C when the phosphorous content in the catalysts was above 0.1 wt%. As the main approaches for introducing P into Cu-containing SSZ-13, impregnation with H_3PO_4 , $(\text{NH}_4)_2\text{HPO}_4$,^{105,108,130} or synthesis of SSZ-13 by using trimethyladamantylammonium hydroxide (TMAdaOH) and tetramethylphosphonium hydroxide (TEPOH) as dual-template agents^{116,152} are reported. Further studies on the influence of phosphorus on the catalytic properties of Cu-SSZ-13 for NH_3 -SCR-De NO_x can be found in ref. 95, 108, 153 and 154. Several researchers suggest that phosphorus tends to poison ZCuOH more easily than Z_2Cu .^{96,155} To regenerate the P-poisoned Cu-SSZ-13 catalysts, phosphorous species in the catalysts should be removed. As an example of that approach, Chen *et al.*⁷¹ successfully applied the combination of washing with hot water (90 °C) and hydrothermal treatment (800 °C for 12 h) to recover the activity of the phosphorous-poisoned Cu-SSZ-13.

Hydrocarbons poisoning

The other aspect associated with the application of NH_3 -SCR-De NO_x is poisoning by hydrocarbons (HCs). The limited DOC activity leads to HCs slipping over the SCR component, which negatively affects its NO_x reduction activity. Therefore, few works regarding the HCs poisoning (carbonaceous deposit, including formed aliphatic compounds: acrolein, acetate and acetone, and aromatic compounds: hydrogen-deficient) effect on Cu-SSZ-13 were reported mainly over C_3H_6 (a representative low-chain HC in the exhaust).^{76,94} For example, Ma *et al.*⁷⁶ found that Cu-SSZ-13 deactivated in the presence of C_3H_6 , due to the competitive adsorption of NH_3 and C_3H_6 on the catalysts as well as blockage of coke in the pore channels. In the case of the aged materials, Wang *et al.*⁹⁴ found that Cu-SSZ-13 (aged at 700 °C) displayed a more severe NO_x conversion decline than the fresh sample in the presence of C_3H_6 . On the other hand, Zhao *et al.*⁹⁷ found that less carbonaceous deposit forms in the



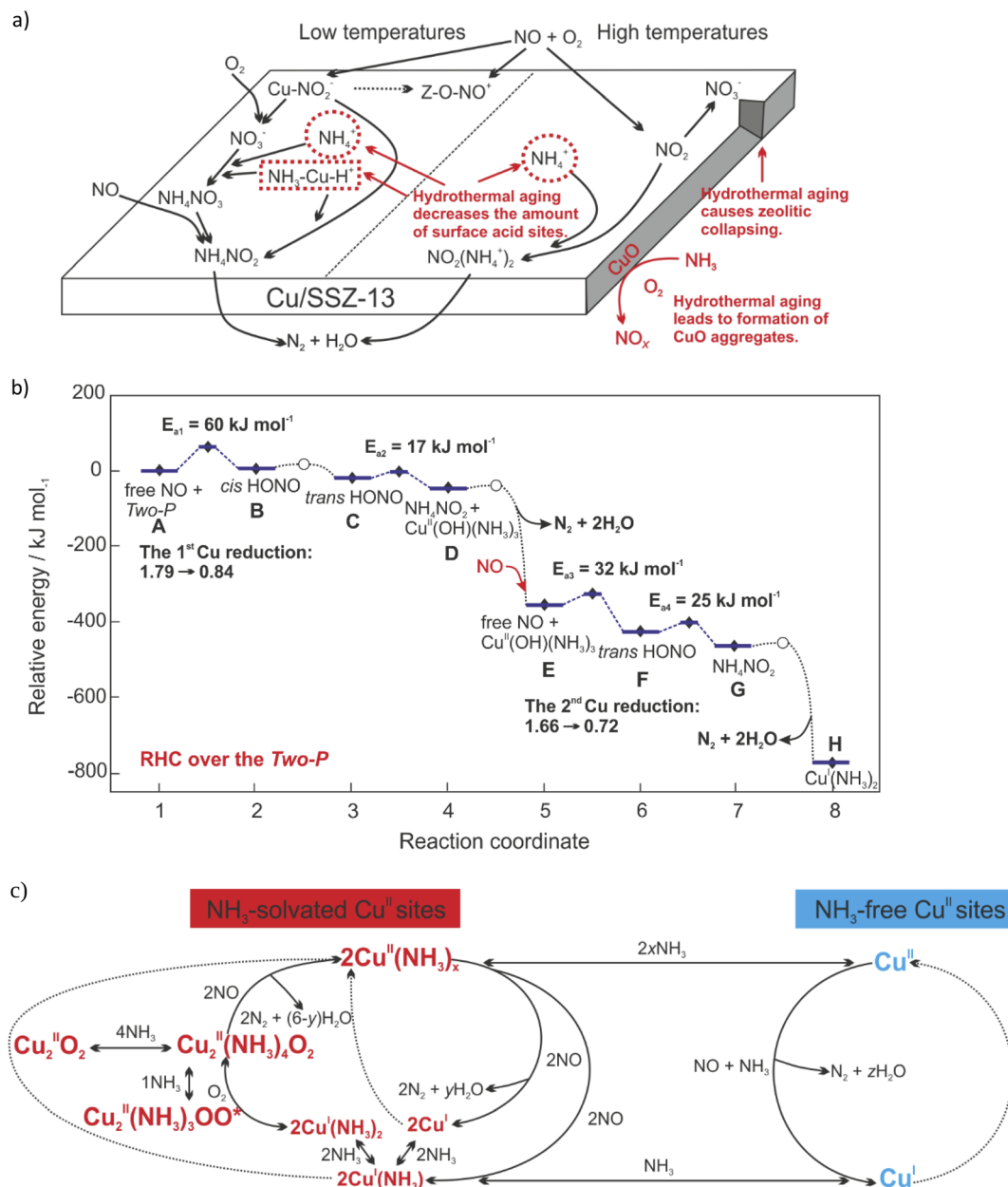


Fig. 5 (a) The influence of hydrothermal aging on the NH_3 -SCR-De NO_x mechanism. Reproduced from ref. 106 with permission from Elsevier, copyright 2019; (b) DFT-computed (HSE06 + D3) energy landscape of LT-RHC over the Two-P. Activation energies and Cu^{II} reduction are reported. $[\text{Cu}^{\text{II}}(\text{OH})(\text{NH}_3)_3 \cdots \text{Cu}^{\text{II}}(\text{OH})(\text{NH}_3)_3]$ stands for the Two-P configuration. Reproduced from ref. 163 with permission from ACS Publications, copyright 2021; (c) Schematic representing the redox of Cu sites during standard NH_3 -SCR-De NO_x . x represents temperature and Cu^{II} speciation-dependent NH_3 solvation of Cu^{II} sites. x range: {1–2}. y represents Cu^{II} speciation-dependent H_2O produced upon the reduction of two NH_3 -solvated Cu^{II} sites. y range: {2–4}. z represents Cu^{II} speciation-dependent H_2O produced upon the reduction of one NH_3 -free Cu^{II} site. z range: {1–2}. Reproduced from ref. 185 with permission from ACS Publications, copyright 2022.

hydrothermally aged samples of Cu-SSZ-13 (due to the lower content of Brønsted acid sites). The presence of aromatic compounds increases with higher HTA temperatures (700, 750, and 800 °C) due to a greater generation of mesopores. Based on these studies, aged Cu-SSZ-13 can prevent the deactivation of Cu-containing SSZ-13 due to HCs poisoning, and thus, maintain its NO activity and stability. Other approaches like hybrid catalysts (e.g., Cu-SSZ-13 with CeO_2 - SnO_2)¹⁰³ were also reported.

Reaction mechanisms

NH_3 -SCR-De NO_x ($4\text{NH}_3 + 4\text{NO} + \text{O}_2 \rightarrow 4\text{N}_2 + 6\text{H}_2\text{O}$) over Cu-containing SSZ-13 can proceed through the adsorption stage of NH_3 and/or NO , according to the Eley-Rideal (E-R; *i.e.*, the gaseous NO reacts with pre-adsorbed NH_3 to produce N_2 and H_2O) and/or Langmuir-Hinshelwood (L-H; both the adsorbed NO and NH_3 simultaneously participate in the reaction) mechanisms.^{23,25,156} For example, the L-H mechanism was

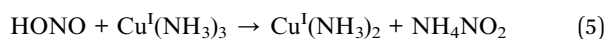
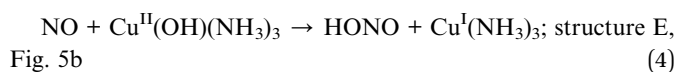
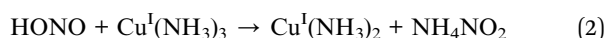
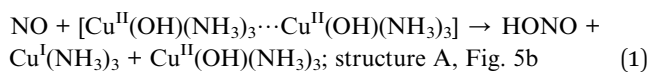


proposed over calcined Cu-SSZ-13, while the E-R mechanism was proposed over its aged form (based on *in situ* DRIFTS analysis). The amount of surface CuO species increased after hydrothermal aging treatment, while the Lewis sites and Brønsted sites (*i.e.*, surface nitrates adsorbed sites and NH₃ capacity) decreased, thus, limiting the formation of intermediate products NH₄NO₃/NH₄NO₂ (below 350 °C) or NO₂(NH₄⁺)₂ (above 350 °C), which in turn led to the loss of NH₃-SCR-DeNO_x activity¹⁰⁶ (Fig. 5a).

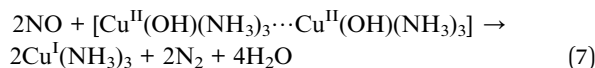
Specifically, NH₃-SCR-DeNO_x on Cu-SSZ-13 follows a redox reaction mechanism, consisting of a reduction half-cycle (RHC; Cu²⁺ → Cu⁺) and an oxidation half-cycle (OHC; Cu⁺ → Cu²⁺). The detailed reaction mechanism is still under debate, indicating the complexity of both RHC and OHC.¹⁵⁷

Reduction half-cycle

When NH₃ is present in the feed, solvation of Z₂Cu with NH₃ is preferred rather than with H₂O,^{158–160} leading to the formation of Cu-amine coordination complexes, *i.e.*, the principal active sites in the redox cycle.^{24,161} The NH₃ solvation of ZCuOH sites (or [Cu₂O₂]²⁺ in their O₂ activated form¹⁶²) may lead to the formation of dimeric or two-proximate Cu-amine complexes (*i.e.*, [Cu^{II}(OH)(NH₃)₃]⁺ units).¹⁶³ NH₃-solvated Z₂Cu sites can hydrolyze to NH₃-solvated ZCuOH sites in the presence of H₂O.¹⁶⁴ Furthermore, the complexes containing a mixture of NH₃ and NO, *i.e.*, [Cu^{II}(OH)(NH₃)_{n-1}(NO)]⁺, were evidenced for the first time by the application of rapid-scan FT-IR spectroscopy and two-dimensional correlation spectroscopy (2D COS) analysis.¹⁶⁵ These solvated Cu moieties were suggested to be active sites in low-temperature NH₃-SCR-DeNO_x (<250 °C).^{51,161} The neighboring NH₃ and NO ligands rearrange to create N-N bonds *via* the formation of nitrosamide (NH₂NO) or ammonium nitrite (NH₄NO₂) intermediates.^{51,161} Subsequently, NH₂NO and NH₄NO₂ decompose into N₂ and H₂O to complete the reduction part of the NH₃-SCR-DeNO_x. As an alternative mechanism, Chen *et al.*^{166,167} proposed the formation of Cu(H₂NNO)²⁺ and Cu(OHNO)²⁺ intermediates that decompose over neighboring Brønsted acid sites to complete the catalytic cycle. The formation of the HONO intermediates was reported also by Usberti *et al.*,¹⁶⁸ who found that activated NO reacted with the NH₃ adsorbed on the Lewis sites (verified also by DFT calculations). This mechanism consists of two sequential NO oxidative activation processes, consisting of NO oxidative activation to HONO catalyzed by [Cu^{II}(OH)(NH₃)₃]⁺, HNO reacting with one NH₃ ligand to NH₄NO₂, and NH₄NO₂ decomposition to N₂ and H₂O¹⁶³ (eqn (1)–(6)):



Summing up the above steps results in a global reaction (eqn (7)):



Thus, Hu *et al.*¹⁶³ and Gramigni *et al.*¹⁶⁹ proved (based on kinetic experimental and DFT calculations) a second-order dependence, suggesting that binuclear reactions between two Cu species could occur during RHC.

The decomposition of NH₄NO₃ (NH₄NO₂ can be oxidized into NH₄NO₃) allows also the side reaction leading to undesired N₂O (<300 °C).⁸⁹ On the other hand, Feng *et al.*¹⁷⁰ claimed that the formation of N₂O resulted from the H₂NNO decomposition over Cu–OOH–Cu complexes, which explains the enhanced N₂O formation with increasing Cu loading. This was further supported by the studies of Xi *et al.*,⁷⁰ who claimed that N₂O formation occur over Cu-oxy species, such as [Cu–O₂–Cu]²⁺. However, N₂O formation has also been reported to mainly occur over [Cu(OH)]⁺ located in CHA cages.^{89,171–173} The high-temperature N₂O production (>300 °C), on the other hand, takes place because of unselective ammonia oxidation. The N₂O production profiles of the different types of SCR catalysts differ considerably.¹¹⁷

Below 250 °C, a linear SCR rate *versus* (Cu loading)² correlation was reported, suggesting that the reaction limiting step involves the participation of two Cu ions.^{54,161} The activation energy for NH₃-SCR-DeNO_x over Cu-containing SSZ-13 varies in the range of 32,¹⁰⁶ 40–41 kJ mol⁻¹,^{54,174} to 43–57 kJ mol⁻¹,¹⁰⁶ also depending on the temperature, *i.e.*, 175–250 °C – 130 kJ mol⁻¹, and 250–300 °C – 60 kJ mol⁻¹.³² Thus, at temperatures above 350 °C, the active sites of Cu-SSZ-13 change from mobile Cu ions coordinated by NH₃ into immobilized Cu ions, thus, giving a seagull profile for NO conversion (based on the Gao *et al.*³² assumptions). Fahami *et al.*⁵³ attributed the activity decrease at around 350 °C to a more localized structure of mono(μ-oxo) dicopper complexes. At high temperatures (above 350 °C), the activity has instead been measured to have a first-order dependence on copper loading, indicating that the reaction can proceed with other possible Cu sites.⁵⁴

Oxidation half-cycle

The [Cu(NH₃)₂]⁺ complexes become the intermediate starting the oxidation half-cycle. The two [Cu^I(NH₃)₂]⁺ intermediates and an oxygen molecules then combine to form [Cu^I(NH₃)₂]⁺–O₂–[Cu^I(NH₃)₂]⁺ intermediates (2[Cu^I(NH₃)₂]⁺ + O₂ → [Cu^I(NH₃)₂]⁺–O₂–[Cu^I(NH₃)₂]⁺).^{51,161,175} The mobility of the Cu ions (*i.e.*, one [Cu^I(NH₃)₂]⁺ must migrate to the vicinity of another; enhanced in the presence of H₂O^{176–178}) guarantees the formation of these dimeric Cu species,^{90,166} thus improving the NH₃-SCR-DeNO_x activity. The 1Al–Cu species (located at isolated single Al sites, *i.e.*, ZCuOH) can form dimeric Cu intermediates more easily than the 2Al–Cu (located at two adjacent Al sites, *i.e.*, Z₂Cu).^{179,180} The ratio of *n*(1Al–Cu)/*n*(2Al–Cu) can be controlled through the catalyst's hydrothermal aging.⁹⁰ Krishna *et al.*¹⁸¹ suggested their



Table 2 Representative results of NH₃-SCO over Cu-containing SSZ-13 reported in the literature

Sample	Preparation method	Reaction conditions	Operation temperature for achieving 100% NH ₃ conversion/ ^o C ((by-)product formation)	Ref.
1	(2.4 wt%)Cu-SSZ-13 ($n(\text{Si})/n(\text{Al}) = 15$) monolith catalyst	Commercial; degreening: 10 vol% O ₂ , 7 vol% H ₂ O, 8 vol% CO ₂ , Ar balance, 550 °C, 4 h	0.02 vol% NH ₃ , 5 vol% O ₂ , 5 vol% H ₂ O, Ar balance, GHSV 40,000 h ⁻¹	72
2	Cu-SSZ-13 (Cu loading, $n(\text{Si})/n(\text{Al})$ not shown) monolith catalyst	Commercial; degreening: 10 vol% O ₂ , 7 vol% H ₂ O, 8 vol% CO ₂ , N ₂ balance, 550–600 °C, 4 h	0.02 vol% NH ₃ , 10 vol% O ₂ , 5 vol% H ₂ O, Ar balance, GHSV 40,000 h ⁻¹	74
3	(2.7 wt%)Cu-SSZ-13 ($n(\text{Si})/n(\text{Al}) = 12$)	Commercial; degreening: 10 vol% H ₂ O, air balance, 650 °C, 12 h; pre-treatment: 21 vol% O ₂ , N ₂ balance, 600 °C, 20 min	0.05 vol% NH ₃ , 5 vol% O ₂ , 3 vol% H ₂ O, N ₂ balance, GHSV 120,000 h ⁻¹	73
Ion-exchange				
4	Cu-SSZ-13 ($n(\text{Si})/n(\text{Al}) = 6$) (Cu content not shown)	Ion-exchange, calcination, 500 °C, 2 h, air	0.035 vol% NH ₃ , 14 vol% O ₂ , 2 vol% H ₂ O, N ₂ balance, GHSV 30,000 h ⁻¹	11
5	(0.88 wt%)Cu-SSZ-13 ($n(\text{Si})/n(\text{Al}) = 25$)	Ion-exchange, calcination, 550 °C, 4 h, air; *hydrothermal treatment: 10 vol% H ₂ O, air balance, 800 °C, 16 h	0.05 vol% NH ₃ , 5 vol% O ₂ , N ₂ balance, GHSV 400,000 h ⁻¹	85
6	(2.1 wt%)Cu-SSZ-13 ($n(\text{Si})/n(\text{Al}) = 12$)	Ion-exchange, calcination conditions not shown; *hydrothermal treatment: 10 vol% H ₂ O, air balance, 550 °C, 16 h	0.036 vol% NH ₃ , 14 vol% O ₂ , 2.5 vol% H ₂ O, N ₂ balance, GHSV 200,000 h ⁻¹	91
7	(2.35 wt%)Cu-SSZ-13 ($n(\text{Si})/n(\text{Al}) = 12.93$)	Ion-exchange, calcination, 550 °C, 4 h, air; pre-treatment: 8 vol% O ₂ , N ₂ balance, 1 h, 500 °C	0.05 vol% NH ₃ , 6.5 vol% O ₂ , 3 vol% H ₂ O, N ₂ balance, GHSV 120,000 h ⁻¹	96
8	(1.88–2.16 wt%)Cu-SSZ-13 ($n(\text{Si})/n(\text{Al}) = 16.5$ –20.3)	Ion-exchange, calcination, 550 °C, 5 h, air; *hydrothermal treatment: 10 vol% H ₂ O, air balance, 750 °C, 16 h; pre-treatment: 21 vol% O ₂ , N ₂ balance, 550 °C, 20 min	0.05 vol% NH ₃ , 5 vol% O ₂ , 3 vol% H ₂ O, N ₂ balance, GHSV 120,000 h ⁻¹	87
9	(4 wt%)Cu-SSZ-13 ($n(\text{Si})/n(\text{Al}) = 11$)	Ion-exchange, calcination conditions not shown; degreening: Reaction conditions, 600 °C, 4 h; pre-treatment: 10 vol% O ₂ , 7 vol% H ₂ O, N ₂ balance, 600 °C, 1 h	0.035 vol% NH ₃ , 10 vol% O ₂ , 7 vol% H ₂ O, N ₂ balance, GHSV 300,000 h ⁻¹	89
10	(4.5–5 wt%)SSZ-13 ($n(\text{Si})/n(\text{Al}) = 9$)	Ion-exchange, calcination, 550 °C, 5 h, air; *hydrothermal treatment: 10 vol% H ₂ O, air balance, 800 °C, 16 h; **degreening: 10 vol% H ₂ O, air balance, 700 °C, 4 h	0.038 vol% NH ₃ , 14 vol% O ₂ , N ₂ balance, GHSV 100,000 h ⁻¹	88
11	(4.76 wt%)Cu-SSZ-13 ($n(\text{Si})/n(\text{Al}) = 4.97$)	Ion-exchange, vacuum evaporator, calcination, 550 °C, 6 h, air	0.1 vol% NH ₃ , 6 vol% O ₂ , He balance, GHSV 300,000 h ⁻¹	195

Table 2 (Contd.)

Sample	Preparation method	Reaction conditions	Operation temperature for achieving 100% NH ₃ conversion/ ^o C ((by)-product formation)	Ref.
One-pot hydrothermal synthesis				
12 (3.5 wt%)Cu-SSZ-13 ($n(\text{Si})/n(\text{Al}) = 6.5$)	One-pot hydrothermal synthesis, HNO ₃ treatment, calcination, 600 °C, 6 h, air; *hydrothermal treatment: 10 vol% H ₂ O, air balance, 750 °C, 16 h	0.05 vol% NH ₃ , 5 vol% O ₂ , N ₂ balance, GHSV 400,000 h ⁻¹	550–600 (not shown), *550–600 (not shown)	106
13 (6.38 wt%)Cu-SSZ-13 ($n(\text{Si})/n(\text{Al}) = 3.77$)	One-pot hydrothermal synthesis, HNO ₃ treatment, calcination, 550 °C, 8 h, air	0.05 vol% NH ₃ , 5 vol% O ₂ , N ₂ balance, *0.05 vol% NH ₃ , 5 vol% O ₂ , 5 vol% H ₂ O, N ₂ balance, GHSV 160,000 h ⁻¹	250–400 (>90% N ₂ selectivity), *300–400 (>90% N ₂ selectivity)	186
Impregnation				
14 (2.2 wt%)Cu-SSZ-13 ($n(\text{Si})/n(\text{Al}) = 12$)	Impregnation, 550 °C, 5 h, air; degreening: 10 vol% H ₂ O, air balance, 650 °C, 4 h; *hydrothermal treatment: 10 vol% H ₂ O, air balance, 800 °C, 16 h Ion-exchange, calcination, 600 °C, 4 h, air	0.036 vol% NH ₃ , 14 vol% O ₂ , 2.5 vol% H ₂ O, N ₂ balance, GHSV 100,000 h ⁻¹	450–550 (not shown), *450–550 (not shown)	118
15 (4.1 wt%)Cu-SSZ-13 ($n(\text{Si})/n(\text{Al}) = 6$) monolith catalyst	Ion-exchange, calcination, 600 °C, 4 h, air	0.04 vol% NH ₃ , 8 vol% O ₂ , 5 vol% H ₂ O, Ar balance, GHSV 22,100 h ⁻¹	450–500 (<3 ppm N ₂ O)	105
16 (10 wt%)Cu-SSZ-13 ($n(\text{Si})/n(\text{Al}) = 10$)	Impregnation, calcination, 550 °C, 6 h, air	0.04 vol% NH ₃ , 10 vol% O ₂ , N ₂ balance, WHSV 300,000 ml g ⁻¹ h ⁻¹	225–450 (>80% N ₂ selectivity)	193

perspective that spatial proximity of active Cu sites is required in the redox cycle of Cu²⁺/Cu⁺. Such proximity assists the oxidation of NH₃-solvated Cu⁺ ions to form dimeric Cu intermediates [Cu^I(NH₃)₂]⁺-O₂-[Cu^I(NH₃)₂]⁺.⁵¹ The structure of mobile dicopper(II) complexes vary depending on the $n(\text{Si})/n(\text{Al})$ ratio of the zeolite host.¹⁸² Finally, the newly formed [Cu^{II}(NH₃)₂]²⁺-O-[Cu^{II}(NH₃)₂]²⁺ hydrolyzes in the presence of H₂O, restoring two [Cu^I(OH)(NH₃)₂]⁺ adducts. O₂ dissociation and NO₂ formation occur on complexes in the presence of NO ([Cu^I(NH₃)₂]⁺-O₂-[Cu^I(NH₃)₂]⁺ + NO → [Cu^{II}(NH₃)₂]²⁺-O²⁻-[Cu^{II}(NH₃)₂]²⁺ + NO₂). Negri *et al.*¹⁸³ proposed (based on combined spectroscopic and DFT studies) that these intermediates are Cu^{II}₂(NH₃)₄O₂ complexes with a side on μ - η^2 , η -peroxo diamino dicopper(II) structure. Besides that, the intermediates were approved *via* DFT calculations and their formation was spectroscopically approved *via* fiber-optic DR UV-Vis spectroscopy during NH₃-SCR-DeNO_x over Cu-containing zeolites.¹⁸⁴ However, the mechanism associated with the reduction of Z₂Cu₂(NH₃)₄O₂ complexes is still unclear. As mentioned above, Paolucci *et al.*¹⁸⁰ claimed that the [Cu^{II}(NH₃)₂]²⁺-O-[Cu^{II}(NH₃)₂]²⁺ hydrolyzes in the presence of H₂O, restoring two [Cu^I(OH)(NH₃)₂]⁺ adducts, thus completing the low-temperature SCR catalytic cycle. However, upon exposure of Z₂Cu₂(NH₃)₄O₂ complexes to NH₃, the formation of unreactive superoxo amino ZCu(NH₃)₃OO* complexes was observed^{183,185} (Fig. 5c). Furthermore, the reaction mechanism changed over field aged (including hydrothermal aging and sulfur aging) Cu-SSZ-13, *i.e.*, lower mobility of the Cu ions coordinated to sulfur-related species led to decreased formation of Cu-dimers necessary for the OHC. The field aging has a minimal impact on RHC.⁷²

Selective ammonia oxidation (NH₃-SCO)

To achieve the desired NO_x conversion, a stoichiometric or even an excess quantity of NH₃ is required, which can result in unreacted NH₃ (also known as NH₃ slip). Thus, oxidation catalysts (ASC, guard catalysts, AMOX) are usually employed to selectively oxidize the unreacted NH₃ (from NH₃-SCR-DeNO_x) into nitrogen and water vapor. Some researchers investigate NH₃-SCO (4NH₃ + 3O₂ → 2N₂ + 6H₂O) as a side process of the NH₃-SCR-DeNO_x, while, there are not many publications dedicated separately to the ammonia oxidation over Cu-containing CHA.^{38,186,187} Similar to NH₃-SCR-DeNO_x, NH₃-SCO is enhanced over Cu-containing catalysts, including zeolite-based catalysts (*e.g.*, Cu-ZSM-5, Cu-Y, Cu-Beta, *etc.*).^{38,188} The aggregated CuO_x species lead to higher NH₃ oxidation,¹¹⁵ thus, across investigated catalytic systems, mainly 10 wt% of Cu loading was found as the optimal.^{188,189} Progress on selective catalytic ammonia oxidation over Cu-containing zeolite-based catalysts was already published by Jabłońska in 2020.³⁸ Furthermore, NH₃-SCO over different catalysts, including proposed reaction mechanisms were reviewed.^{188–190} Thus, in this chapter, there is a focus on the Cu-containing SSZ-13 based-catalysts prepared *via* different techniques *i.e.*, containing different amounts of Cu species.



Table 2 lists representative results of NH_3 -SCO over Cu-containing SSZ-13 reported in the literature. For example, Gao *et al.*³² found that NH_3 conversion increases with higher Cu loading (exchange level 23–90%), which possibly arises from the weaker interactions between Cu^{2+} ions and the SSZ-13 framework (*i.e.*, more facile $\text{Cu}^{2+} \leftrightarrow \text{Cu}^+$ redox-cycling) or higher amount of Cu^{2+} ions placed closer to the pore openings (being more accessible to reactants). Similar to the NH_3 -SCR-DeNO_x, the authors observed the seagull profile of NH_3 conversion, which was later also approved by Olsson *et al.*^{191,192} These two regimes, below and above 250 °C (400 °C in ref. 191) with different values of activation energy over Cu-SSZ-13 were attributed to the change in the catalytic centers resulting in a different activity. Cui *et al.*⁸⁸ reported a higher activity for Cu/SSZ-13 with increasing Cu loading up to 5 wt% (Fig. 6a). After hydrothermal aging (at 800 °C for 16 h) the full NH_3 conversion is shifted about 50 °C higher (Table 2, pos. 10). In another example, NH_3 oxidation activity decreases with increasing HTA temperature (550–900 °C). The activity decrease was assigned to the loss of active isolated Cu^{2+} species (active below 400 °C) during aging, and a decrease in NH_3 storage capacity.⁹¹ Both Cu^{2+} ions and CuO coexist in Cu/SSZ-13 ($n(\text{Si})/n(\text{Al}) = 16$ –24) prepared by impregnation.¹⁹³ Enhanced activity over Cu/SSZ-13 with $n(\text{Si})/n(\text{Al}) = 20$ (activation energy of 68 kJ mol⁻¹) resulted from the highest content of CuO species and acid sites (Fig. 6b). Contrary to that, Han *et al.*⁸⁰ reported no significant changes for

Cu-SSZ-13 with a $n(\text{Si})/n(\text{Al})$ ratio of 5.5 (among 11, 21) in NH_3 conversion for the whole temperature range. However, the NO_x conversion slightly increased from 10 to 20 ppm at 625 °C after hydrothermal aging at 800 °C. Based on the *in situ* DRIFTS, the authors claimed that NH_3 -SCO over Cu/SSZ-13 follows the *in situ*/internal SCR (i-SCR) mechanism, consisting of two steps. In the first step, NH_3 was oxidized to NO_x by surface CuO. Subsequently, NO_x was reduced to N_2 and H_2O by unreacted NH_3 on isolated Cu^{2+} sites (*i.e.*, NH_3 -SCR-DeNO_x).¹⁹³ Thus, Cu-SSZ-13 revealed higher NH_3 oxidation than CuO/SSZ-13 (CuO mechanically mixed with SSZ-13).⁸⁷ A similar conclusion about the reaction mechanism was given over Cu-SSZ-13 (prepared by one-pot hydrothermal synthesis) treated with dilute HNO_3 solution.¹⁸⁶ The reaction mechanism was assigned based on the *in situ* DRIFTS studies, excluding the hydrazine mechanism (as the N_2H_4 species were not observed in the spectra). Details on the reaction mechanisms can be found elsewhere.^{188,189,194} The one-pot synthesized Cu-SSZ-13 treated with dilute HNO_3 possessed added Cu^{2+} ions that accelerated low-temperature NH_3 -SCR-DeNO_x (second step of NH_3 -SCO). Thus, enhanced activity and N_2 selectivity over this catalyst were reported (Fig. 6c) compared to non-modified zeolite-based catalysts. One-pot hydrothermally prepared Cu-SSZ-13 ($n(\text{Si})/n(\text{Al}) = 6.5$ –12.5, 1.8–3.5 wt% of Cu) did not show significant changes before and after the hydrothermal aging treatment (Table 2, pos. 12) in the whole temperature range.¹⁰⁶ However, Luo *et al.*⁷⁴ have shown

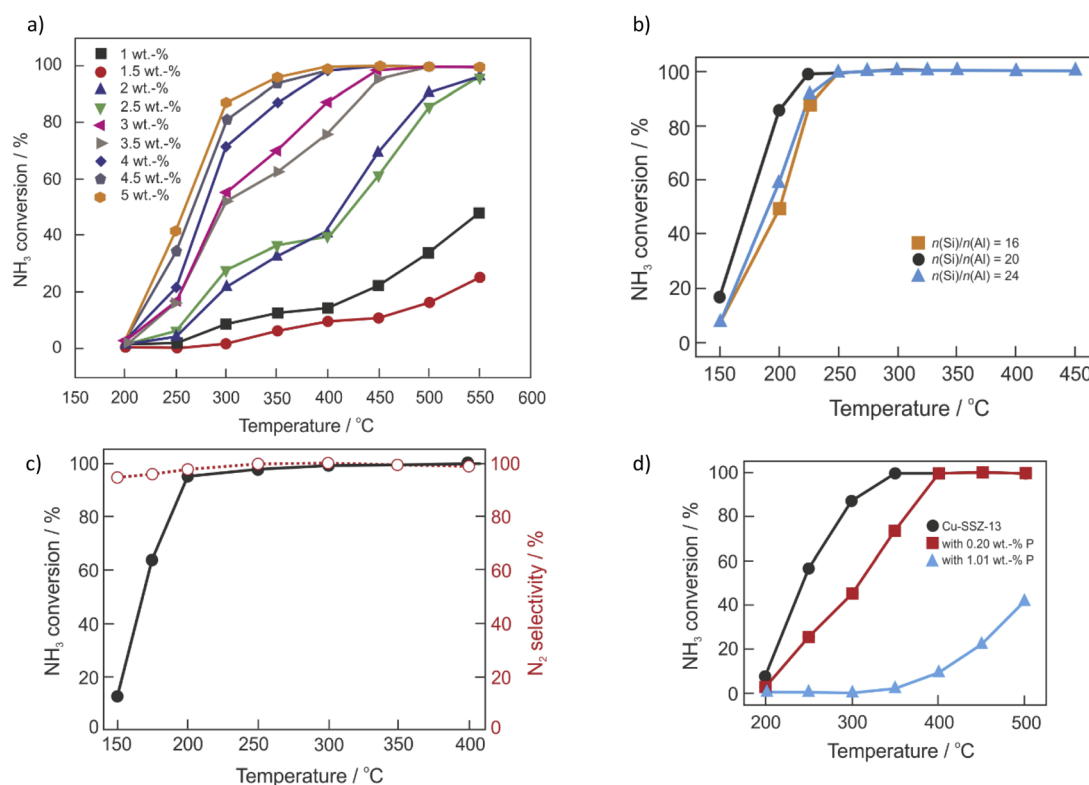


Fig. 6 (a) NH_3 conversion over degreened Cu/H-SSZ-13. Reproduced from ref. 88 with permission from Elsevier, copyright 2020; (b) NH_3 conversion over Cu/SSZ-13 with different $n(\text{Si})/n(\text{Al})$ ratios. Reproduced from ref. 193 with permission from Elsevier, copyright 2020; (c) NH_3 conversion over Cu-SSZ-13 post-modified with a solution of HNO_3 . Reproduced from ref. 186 with permission from ACS Publications, copyright 2018; (d) NH_3 conversion over fresh and P-poisoned Cu-SSZ-13. Reproduced from ref. 96 with permission from ACS Publications, copyright 2021.



that NH₃ oxidation activity of commercial Cu-SSZ-13 (detail of composition or preparation not shown) decreases with increased temperature up to 800 °C. Cu-SSZ-13 – prepared *via* the solid-state ion-exchange method at 700–800 °C, did not reach full conversion.¹¹⁵ On the other hand, the enhanced activity of bifunctional catalysts was reported, with single examples given as mixed, dual-layer and hybrid layer designs composed of Pt/Al₂O₃ and Cu-SSZ-13,^{196–198} or Ru/Cu-SSZ-13.¹⁹⁹ Similar to Cu-containing SSZ-13 applied in NH₃-SCR-DeNO_x, also the catalysts applied in NH₃-SCO lost their activity after poisoning, *e.g.*, with P^{96,105} (Fig. 6d). Catalyst activity decreased remarkably with P loading (0.26–1.21 wt%) and especially above 300 °C, because of the interaction between phosphorus with oligomeric Cu_xO_y species inside the large cages. As these species are not active in NH₃-SCR-DeNO_x the effect is less pronounced, as reported before.¹⁰⁵

Conclusions and perspectives

This review summarizes recent progress in the NH₃-SCR-DeNO_x and the NH₃-SCO over Cu-containing SSZ-13 catalysts, concerning their preparation methods, hydrothermal stability and poisoning, as well as their reaction mechanisms. Various preparation methods have been applied to manipulate the nature and distribution of Cu species in the materials, with continuous efforts aiming at improving the (hydrothermal) stability of the Cu-CHA catalysts. Minimizing [Cu(OH)]⁺-Z sites, which are more susceptible to hydrothermal aging, sulfur or phosphorus poisoning than Cu²⁺-2Z, will be a challengeable task in the following years. Determining the effect of (new) dopants on catalyst stability is a promising research direction. Furthermore, more work should be spent on the application of the degreening and treatment/poisoning strategies closely related to the industrial applications (*i.e.*, degreening at 700 °C in 10 vol% O₂, 5 vol% of CO₂ and H₂O, followed by the aging at 800 °C for 50 h for diesel exhaust applications).²⁰⁰ Besides enhanced activity and stability, N₂ selectivity also indicates the commercialization of catalysts. Despite recent findings, an accurate and experimentally established standard NH₃-SCR-DeNO_x reaction mechanisms at low temperatures including field aged materials is still missing. Thus, more detailed *in situ* and operando studies, transient kinetic investigations, as well as molecular-scale computational models, are required to further understand reaction mechanisms.

Furthermore, compared to NH₃-SCR-DeNO_x, the studies of NH₃-SCO are rather scarce. Mainly, ammonia oxidation is considered as the side process of NH₃-SCR-DeNO_x above 350–400 °C. The catalytic experiments have been conducted under conditions, which differ far from the ones existing in the diesel aftertreatment system, *i.e.*, minor NH₃ slip (O₂ excess), presence of H₂O, CO_x or SO_x, *etc.* Besides, key requirements comprehend high activity and N₂ selectivity up to 600–700 °C (in the cycle of diesel particulate filter regeneration) and stability under application-relevant reaction conditions. A limited amounts of studies focus on the investigation of the reaction mechanisms. Furthermore, there are no systematic studies on the development of bifunctional catalysts. As NH₃-

SCO proceeds mainly according to the i-SCR mechanism (*i.e.*, with NH₃-SCR-DeNO_x as the second step), similar reaction paths can be potentially ascribed for a description of the activity of Cu-containing SSZ-13. Thus, more effort must be spent on studying NH₃-SCO reaction mechanisms in the future. Systematic studies (*i.e.*, careful design, appropriate coupling techniques, *etc.*) should also cover bifunctional catalysts composed of Cu-containing SSZ-13 (NH₃-SCR-DeNO_x function) and noble metal-based catalyst (NH₃ oxidation function). A collective understanding of reaction and deactivation mechanisms of both components allows for the design of high-performing NH₃-SCO catalysts with appropriate catalyst promotion strategies. Thus, the development of such hybrid catalysts (in monolith form) for diesel exhaust aftertreatment systems is a topic of interest.

Conflicts of interest

There are no conflicts to declare.

Acknowledgements

M. J. acknowledges a DFG Research Grant JA 2998/2-1 and support from Universität Leipzig for Open Access Publishing.

References

- 1 R. Chen, T. Zhang, Y. Guo, J. Wang, J. Wei and Q. Yu, *Chem. Eng. J.*, 2021, **420**, 127588–127631.
- 2 M. Jabłońska and L. Chmielarz, *Zesz. Nauk.*, 2013, **7**, 7–23.
- 3 T. Boningari and P. G. Smirniotis, *Curr. Opin. Chem. Eng.*, 2016, **13**, 133–141.
- 4 C. Rusznak, S. Jenkins, P. R. Mills, R. J. Sapsford, J. L. Devalia and R. J. Davies, *Rev. Fr. d'Allergologie d'Immunologie Clin.*, 1998, **38**, S80–S90.
- 5 X. Wang, Y. Xu, Z. Zhao, J. Liao, C. Chen and Q. Li, *Fuel*, 2021, **305**, 121482–121501.
- 6 T. Andana, K. G. Rappé, F. Gao, J. Szanyi, X. Pereira-Hernandez and Y. Wang, *Appl. Catal., B*, 2021, 120054–120079.
- 7 Y. Zeng, K.-G. Haw, Y. Wang, S. Zhang, Z. Wang, Q. Zhong and S. Kawi, *ChemCatChem*, 2021, **13**, 491–505.
- 8 M. Iwamoto, H. Furukawa, Y. Mine, F. Uemura, S. Mikuriya and S. Kagawa, *J. Chem. Soc., Chem. Commun.*, 1986, 1272–1273.
- 9 A. Wang, Y. Chen, E. D. Walter, N. M. Washton, D. Mei, T. Varga, Y. Wang, J. Szanyi, Y. Wang, C. H. F. Peden and F. Gao, *Nat. Commun.*, 2019, **10**, 1–10.
- 10 Q. Ye, L. Wang and R. T. Yang, *Appl. Catal., A*, 2012, **427**, 24–34.
- 11 J. H. Kwak, R. G. Tonkyn, D. H. Kim, J. Szanyi and C. H. F. Peden, *J. Catal.*, 2010, **275**, 187–190.
- 12 D. W. Fickel and R. F. Lobo, *J. Phys. Chem. C*, 2010, **114**, 1633–1640.
- 13 C. Baerlocher, L. B. McCusker and D. H. Olson, *Atlas of zeolite framework types*, Elsevier, 2007, pp. 96–97.



- 14 S. Prodinge, M. A. Derewinski, Y. Wang, N. M. Washton, E. D. Walter, J. Szanyi, F. Gao, Y. Wang and C. H. F. Peden, *Appl. Catal., B*, 2017, **201**, 461–469.
- 15 S. I. Zones, *US Pat.* 4544538, 1985.
- 16 B. Chen, R. Xu, R. Zhang and N. Liu, *Environ. Sci. Technol.*, 2014, **48**, 13909–13916.
- 17 R. Xu, R. Zhang, N. Liu, B. Chen and S. Zhang Qiao, *ChemCatChem*, 2015, **7**, 3842–3847.
- 18 X. Wang, Q. Wu, C. Chen, S. Pan, W. Zhang, X. Meng, S. Maurer, M. Feyen, U. Müller and F.-S. Xiao, *Chem. Commun.*, 2015, **51**, 16920–16923.
- 19 D. W. Fickel, E. D'Addio, J. A. Lauterbach and R. F. Lobo, *Appl. Catal., B*, 2011, **102**, 441–448.
- 20 J. H. Kwak, D. Tran, S. D. Burton, J. Szanyi, J. H. Lee and C. H. F. Peden, *J. Catal.*, 2012, **287**, 203–209.
- 21 S. J. Schmiege, S. H. Oh, C. H. Kim, D. B. Brown, J. H. Lee, C. H. F. Peden and D. H. Kim, *Catal. Today*, 2012, **184**, 252–261.
- 22 Y. Shan, J. Du, Y. Zhang, W. Shan, X. Shi, Y. Yu, R. Zhang, X. Meng, F.-S. Xiao and H. He, *Natl. Sci. Rev.*, 2021, **8**, nwab010.
- 23 J. Wang, H. Zhao, G. Haller and Y. Li, *Appl. Catal., B*, 2017, **202**, 346–354.
- 24 F. Gao and F. Peden, *Catalysts*, 2018, **18**, 140–163.
- 25 A. M. Beale, F. Gao, I. Lezcano-Gonzalez, C. H. F. Peden and J. Szanyi, *Chem. Soc. Rev.*, 2015, **44**, 7371–7405.
- 26 Y. Xin, Q. Li and Z. Zhang, *ChemCatChem*, 2018, **10**, 29–41.
- 27 S. Zhang, L. Pang, Z. Chen, S. Ming, Y. Dong, Q. Liu, P. Liu, W. Cai and T. Li, *Appl. Catal., A*, 2020, **607**, 117855–117876.
- 28 J. H. Kwak, H. Zhu, J. H. Lee, C. H. F. Peden and J. Szanyi, *Chem. Commun.*, 2012, **48**, 4758–4760.
- 29 F. Giordanino, P. N. R. Vennestrom, L. F. Lundegaard, F. N. Stappen, S. Mossin, P. Beato, S. Bordiga and C. Lamberti, *Dalton Trans.*, 2013, **42**, 12741–12761.
- 30 X. Wang, Y. Xu, M. Qin, Z. Zhao, X. Fan and Q. Li, *J. Colloid Interface Sci.*, 2022, **622**, 1–10.
- 31 S. T. Korhonen, D. W. Fickel, R. F. Lobo, B. M. Weckhuysen and A. M. Beale, *Chem. Commun.*, 2011, **47**, 800–802.
- 32 F. Gao, E. D. Walter, E. M. Karp, J. Luo, R. G. Tonkyn, J. H. Kwak, J. Szanyi and C. H. F. Peden, *J. Catal.*, 2013, **300**, 20–29.
- 33 Y. J. Kim, J. K. Lee, K. M. Min, S. B. Hong, I.-S. Nam and B. K. Cho, *J. Catal.*, 2014, **311**, 447–457.
- 34 A. Godiksen, F. N. Stappen, P. N. R. Vennestrom, F. Giordanino, S. B. Rasmussen, L. F. Lundegaard and S. Mossin, *J. Phys. Chem. C*, 2014, **118**, 23126–23138.
- 35 G. Centi and S. Perathoner, *Appl. Catal., A*, 1995, **132**, 179–259.
- 36 S. A. Bates, A. A. Verma, C. Paolucci, A. A. Parekh, T. Anggara, A. Yezerets, W. F. Schneider, J. T. Miller, W. N. Delgass and F. H. Ribeiro, *J. Catal.*, 2014, **312**, 87–97.
- 37 A. A. Verma, S. A. Bates, T. Anggara, C. Paolucci, A. A. Parekh, K. Kamasamudram, A. Yezerets, J. T. Miller, W. N. Delgass, W. F. Schneider and F. H. Ribeiro, *J. Catal.*, 2014, **312**, 179–190.
- 38 M. Jabłońska, *ChemCatChem*, 2020, **12**, 4490–4500.
- 39 J. Dědeček, B. Wichterlova and P. Kubat, *Microporous Mesoporous Mater.*, 1999, **32**, 63–74.
- 40 M. Zamadics, X. Chen and L. Kevan, *J. Phys. Chem.*, 1992, **96**, 2652–2657.
- 41 X. Yang, Z. Wu, M. Moses-Debusk, D. R. Mullins, S. M. Mahurin, R. A. Geiger, M. Kidder and C. K. Narula, *J. Phys. Chem. C*, 2012, **116**, 23322–23331.
- 42 T. Zhang, J. Li, J. Liu, D. Wang, Z. Zhao, K. Cheng and J. Li, *AIChE J.*, 2015, **61**, 3825–3837.
- 43 Y. Wang, L. Xie, F. Liu and W. Ruan, *J. Environ. Sci.*, 2019, **81**, 195–204.
- 44 Y. Yue, B. Liu, P. Qin, N. Lv, T. Wang, X. Bi, H. Zhu, P. Yuan, Z. Bai, Q. Cui and X. Bao, *Chem. Eng. J.*, 2020, **398**, 125515–125527.
- 45 J. Du, J. Wang, X. Shi, Y. Shan, Y. Zhang and H. He, *Catalysts*, 2020, **10**, 1375–1389.
- 46 Z. Wang, X. Xu, Y. Zhu, H. He, N. Wang, X. Yang and L. Liu, *Microporous Mesoporous Mater.*, 2022, **333**, 111720–111729.
- 47 S. Zhang, J. Chen, Y. Meng, L. Pang, Y. Guo, Z. Luo, Y. Fang, Y. Dong, W. Cai and T. Li, *Appl. Surf. Sci.*, 2022, **571**, 151328–151341.
- 48 D. He, Z. Wang, D. Deng, S. Deng, H. He and L. Liu, *Mol. Catal.*, 2020, **484**, 110738–110748.
- 49 F. Gao, N. M. Washton, Y. Wang, M. Kollár, J. Szanyi and C. H. F. Peden, *J. Catal.*, 2015, **331**, 25–38.
- 50 Z. Liu, T. Wakihara, K. Oshima, D. Nishioka, Y. Hotta, S. P. Elangovan, Y. Yanaba, T. Yoshikawa, W. Chaikittisilp, T. Matsuo, T. Takewaki and T. Okubo, *Angew. Chem.*, 2015, **127**, 5775–5779.
- 51 F. Gao, D. Mei, Y. Wang, J. Szanyi and C. H. F. Peden, *J. Am. Chem. Soc.*, 2017, **139**, 4935–4942.
- 52 S. Dahlin, J. Englund, H. Malm, M. Feigel, B. Westerberg, F. Regali, M. Skoglundh and L. J. Pettersson, *Catal. Today*, 2021, **360**, 326–339.
- 53 A. R. Fahami, T. Günter, D. E. Doronkin, M. Casapu, D. Zengel, T. H. Vuong, M. Simon, F. Breher, A. V. Kucherov, A. Brückner and J.-D. Grunwaldt, *React. Chem. Eng.*, 2019, **4**, 1000–1018.
- 54 F. Gao, E. D. Walter, M. Kollar, Y. Wang, J. Szanyi and C. H. F. Peden, *J. Catal.*, 2014, **319**, 1–14.
- 55 M. Rutkowska, I. Pacia, S. Basağ, A. Kowalczyk, Z. Piwowarska, K. A. Duda Michałand Tarach, K. Góra-Marek, M. Michalik, U. Díaz and L. Chmielarz, *Microporous Mesoporous Mater.*, 2017, **246**, 193–206.
- 56 R. S. R. Suharbiansah, K. Pyra, M. Liebau, D. Poppitz, K. Góra-Marek, R. Gläser and M. Jabłońska, *Microporous Mesoporous Mater.*, 2022, **334**, 111793–111804.
- 57 M. Jabłońska, K. Góra-Marek, M. Grilc, P. C. Bruzzese, D. Poppitz, K. Pyra, M. Liebau, A. Pöpl, B. Likozar and R. Gläser, *Catalysts*, 2021, **11**, 843–870.
- 58 R. Oord, I. C. Ten Have, J. M. Arends, F. C. Hendriks, J. Schmidt, I. Lezcano-Gonzalez and B. M. Weckhuysen, *Catal. Sci. Technol.*, 2017, **7**, 3851–3862.
- 59 G. Wu, S. Liu, Z. Chen, Q. Yu, Y. Chu, H. Xiao, H. Peng, D. Fang, S. Deng and Y. Chen, *J. Taiwan Inst. Chem. Eng.*, 2022, **134**, 104355–104367.



- 60 H. Jiang, B. Guan, X. Peng, R. Zhan, H. Lin and Z. Huang, *Chem. Eng. J.*, 2020, **379**, 122358–122373.
- 61 L. Ren, L. Zhu, C. Yang, Y. Chen, Q. Sun, H. Zhang, C. Li, F. Nawaz, X. Meng and F.-S. Xiao, *Chem. Commun.*, 2011, **47**, 9789–9791.
- 62 R. Martínez-Franco, M. Moliner, J. R. Thogersen and A. Corma, *ChemCatChem*, 2013, **5**, 3316–3323.
- 63 C. Fan, Z. Chen, L. Pang, S. Ming, X. Zhang, K. B. Albert, P. Liu, H. Chen and T. Li, *Appl. Catal., A*, 2018, **550**, 256–265.
- 64 J. Han, X. Jin, C. Song, Y. Bi, Q. Liu, C. Liu, N. Ji, X. Lu, D. Ma and Z. Li, *Green Chem.*, 2020, **22**, 219–229.
- 65 J. Feng, D. Shi, Z. Xu, J. Wang, Y. Wang and X. Li, *Russ. J. Phys. Chem. A*, 2020, **94**, 1797–1803.
- 66 B. Liu, N. Lv, C. Wang, H. Zhang, Y. Yue, J. Xu, X. Bi and X. Bao, *Chin. J. Chem. Eng.*, 2022, **41**, 329–341.
- 67 L. Xie, F. Liu, L. Ren, X. Shi, F.-S. Xiao and H. He, *Environ. Sci. Technol.*, 2014, **48**, 566–572.
- 68 L. Ma, Y. Cheng, G. Cavataio, R. W. McCabe, L. Fu and J. Li, *Chem. Eng. J.*, 2013, **225**, 323–330.
- 69 Y. Xi, C. Su, N. A. Ottinger and Z. G. Liu, *Appl. Catal., B*, 2021, **284**, 119749–119759.
- 70 Y. Xi, N. A. Ottinger, C. J. Keturakis and Z. G. Liu, *Appl. Catal., B*, 2021, **294**, 120245–120257.
- 71 Z. Chen, C. Bian, Y. Guo, L. Pang and T. Li, *ACS Catal.*, 2021, **11**, 12963–12976.
- 72 D. J. Deka, R. Daya, A. Ladshaw, D. Trandal, S. Y. Joshi and W. P. Partridge, *Appl. Catal., B*, 2022, **309**, 121233–121248.
- 73 Y. Ma, Z. Shao, X. Wu, Y. Gao, B. Jin, R. Ran, Z. Si, Z. Li and D. Weng, *React. Chem. Eng.*, 2022, DOI: [10.1039/d2re00140c](https://doi.org/10.1039/d2re00140c).
- 74 J. Luo, H. An, K. Kamasamudram, N. Currier, A. Yezerets, T. Watkins and L. Allard, *SAE Int. J. Engines*, 2015, **8**, 1181–1186.
- 75 J. Luo, D. Wang, A. Kumar, J. Li, K. Kamasamudram, N. Currier and A. Yezerets, *Catal. Today*, 2016, **267**, 3–9.
- 76 L. Ma, W. Su, Z. Li, J. Li, L. Fu and J. Hao, *Catal. Today*, 2015, **245**, 16–21.
- 77 F. Gao, Y. Wang, N. M. Washton, M. Kollar, J. Szanyi and C. H. F. Peden, *ACS Catal.*, 2015, **5**, 6780–6791.
- 78 T. Ryu, H. Kim and S. B. Hong, *Appl. Catal., B*, 2019, **245**, 513–521.
- 79 R. Oord, J. E. Schmidt and B. M. Weckhuysen, *Catal. Sci. Technol.*, 2018, **8**, 1028–1038.
- 80 S. Han, J. Cheng, C. Zheng, Q. Ye, S. Cheng, T. Kang and H. Dai, *Appl. Surf. Sci.*, 2017, **419**, 382–392.
- 81 J. Wang, L. Shao, C. Wang, J. Wang, M. Shen and W. Li, *J. Catal.*, 2018, **367**, 221–228.
- 82 Z. Zhao, R. Yu, R. Zhao, C. Shi, H. Gies, F.-S. Xiao, D. De Vos, T. Yokoi, X. Bao, U. Kolb, M. Feyen, R. McGuire, S. Maurer, A. Moini, U. Müller and W. Zhang, *Appl. Catal., B*, 2017, **217**, 421–428.
- 83 Y. Zhang, Y. Peng, J. Li, K. Groden, J.-S. McEwen, E. D. Walter, Y. Chen, Y. Wang and F. Gao, *ACS Catal.*, 2020, **10**, 9410–9419.
- 84 J. Liang, Y. Mi, G. Song, H. Peng, Y. Li, R. Yan, W. Liu, Z. Wang, P. Wu and F. Liu, *J. Hazard. Mater.*, 2020, **398**, 122986–122998.
- 85 Z. Liu, B. Guan, H. Jiang, Y. Wei, X. Wu, J. Zhou, H. Lin and Z. Huang, *New J. Chem.*, 2022, **46**, 13593–13608.
- 86 J. Zhang, J. Liang, H. Peng, Y. Mi, P. Luo, H. Xu, M. He and P. Wu, *Appl. Catal., B*, 2021, **292**, 120163–120175.
- 87 Y. Ma, S. Cheng, X. Wu, T. Ma, L. Liu, B. Jin, M. Liu, J. Liu, R. Ran, Z. Si and D. Weng, *J. Catal.*, 2022, **405**, 199–211.
- 88 Y. Cui, Y. Wang, E. D. Walter, J. Szanyi, Y. Wang and F. Gao, *Catal. Today*, 2020, **339**, 233–240.
- 89 D. Yao, B. Liu, F. Wu, Y. Li, X. Hu, W. Jin and X. Wang, *Ind. Eng. Chem. Res.*, 2021, **60**, 10083–10093.
- 90 H. Lee, I. Song, S. W. Jeon and D. H. Kim, *J. Phys. Chem. Lett.*, 2021, **12**, 3210–3216.
- 91 J. Song, Y. Wang, E. D. Walter, N. M. Washton, D. Mei, L. Kovarik, M. H. Engelhard, S. Prodingler, Y. Wang, C. H. F. Peden and F. Gao, *ACS Catal.*, 2017, **7**, 8214–8227.
- 92 Y. Shan, X. Shi, J. Du, Z. Yan, Y. Yu and H. He, *Ind. Eng. Chem. Res.*, 2019, **58**, 5397–5403.
- 93 H. Al Jabri, K. Miyake, K. Ono, M. Nakai, R. Inoue, Y. Hirota, Y. Uchida, Y. Wang, T. Nishitoba, T. Yokoi, T. Ohnishi, M. Ogura and N. Nishiyama, *Microporous Mesoporous Mater.*, 2020, **297**, 109780–109786.
- 94 A. Wang, Y. Wang, E. D. Walter, N. M. Washton, Y. Guo, G. Lu, C. H. F. Peden and F. Gao, *Catal. Today*, 2019, **320**, 91–99.
- 95 Z. Chen, C. Fan, L. Pang, S. Ming, P. Liu and T. Li, *Appl. Catal., B*, 2018, **237**, 116–127.
- 96 A. Guo, K. Xie, H. Lei, V. Rizzotto, L. Chen, M. Fu, P. Chen, Y. Peng, D. Ye and U. Simon, *Environ. Sci. Technol.*, 2021, **55**, 12619–12629.
- 97 H. Zhao, X. Wu, Z. Huang, H. Shen, J. Dong, X. Li and G. Jing, *Energy Fuels*, 2022, **36**, 2712–2721.
- 98 H. Zhao, M. Lin, Y. Wang and J. Zheng, *RSC Adv.*, 2021, **11**, 33334–33343.
- 99 M. Chen, Y. Wei, J. Han, W. Yan and J. Yu, *Mater. Chem. Front.*, 2021, **5**, 7787–7795.
- 100 M.-J. Han, Y.-L. Jiao, C.-H. Zhou, Y.-L. Guo, Y. Guo, G.-Z. Lu, L. Wang and W.-C. Zhan, *Rare Met.*, 2019, **38**, 210–220.
- 101 Z. Zhao, R. Yu, C. Shi, H. Gies, F.-S. Xiao, D. De Vos, T. Yokoi, X. Bao, U. Kolb, R. McGuire, A.-N. Parvulescu, S. Maurer, U. Müller and W. Zhang, *Catal. Sci. Technol.*, 2019, **9**, 241–251.
- 102 Y. Cui, Y. Wang, D. Mei, E. D. Walter, N. M. Washton, J. D. Holladay, Y. Wang, J. Szanyi, C. H. F. Peden and F. Gao, *J. Catal.*, 2019, **378**, 363–375.
- 103 F. Martinovic, F. A. Deorsola, M. Armandi, B. Bonelli, R. Palkovits, S. Bensaid and R. Pirone, *Appl. Catal., B*, 2021, **282**, 119536–119549.
- 104 T. Usui, Z. Liu, S. Ibe, J. Zhu, C. Anand, H. Igarashi, N. Onaya, Y. Sasaki, Y. Shiramata, T. Kusamoto and T. Wahikara, *ACS Catal.*, 2018, **8**, 9165–9173.
- 105 K. Xie, K. Leistner, K. Wijayanti, A. Kumar, K. Kamasamudram and L. Olsson, *Catal. Today*, 2017, **297**, 46–52.
- 106 H. Jiang, B. Guan, H. Lin and Z. Huang, *Fuel*, 2019, **255**, 115587–115604.
- 107 H. Zhao, L. Han, Y. Wang and J. Zheng, *Catalysts*, 2021, **11**, 796–806.



- 108 H. Zhao, Y. Zhao, M. Liu, X. Li, Y. Ma, X. Yong, H. Chen and Y. Li, *Appl. Catal., B*, 2019, **252**, 230–239.
- 109 R. Xu, Z. Wang, N. Liu, C. Dai, J. Zhang and B. Chen, *ACS Catal.*, 2020, **10**, 6197–6212.
- 110 Y. Shan, J. Du, Y. Yu, W. Shan, X. Shi and H. He, *Appl. Catal., B*, 2020, **266**, 118655–118667.
- 111 X. Wang, Y. Sun, F. Han and Y. Zhao, *J. Environ. Chem. Eng.*, 2022, 107888–107898.
- 112 S. Shwan, M. Skoglundh, L. F. Lundegaard, R. R. Tiruvalam, T. V. W. Janssens, A. Carlsson and P. N. R. Vennestrøm, *ACS Catal.*, 2015, **5**, 16–19.
- 113 A. K. S. Clemens, A. Shishkin, P.-A. Carlsson, M. Skoglundh, F. J. Martínez-Casado, Z. Matej, O. Balmes and H. Harelind, *ACS Catal.*, 2015, **5**, 6209–6218.
- 114 L. Xie, F. Liu, X. Shi, F.-S. Xiao and H. He, *Appl. Catal., B*, 2015, **179**, 206–212.
- 115 D. Wang, F. Gao, C. H. F. Peden, J. Li, K. Kamasamudram and W. S. Epling, *ChemCatChem*, 2014, **6**, 1579–1583.
- 116 Y. Yamasaki, N. Tsunooji, Y. Takamitsu, M. Sadakane and T. Sano, *Microporous Mesoporous Mater.*, 2016, **223**, 129–139.
- 117 J. Han, A. Wang, G. Isapour, H. Harelind, M. Skoglundh, D. Creaser and L. Olsson, *Ind. Eng. Chem. Res.*, 2021, **60**, 17826–17839.
- 118 B. Peng, K. G. Rappé, Y. Cui, F. Gao, J. Szanyi, M. J. Olszta, E. D. Walter, Y. Wang, J. D. Holladay and R. A. Goffe, *Appl. Catal., B*, 2020, **263**, 118359–118370.
- 119 L. Xie, F. Liu, K. Liu, X. Shi and H. He, *Catal. Sci. Technol.*, 2014, **4**, 1104–1110.
- 120 M. Jabłońska, *Mol. Catal.*, 2022, **518**, 112111–112132.
- 121 P. N. R. Vennestrøm, L. F. Lundegaard, C. Tyrsted, D. A. Bokarev, A. I. Mytareva, G. N. Baeva, A. Y. Stakheev and T. V. W. Janssens, *Top. Catal.*, 2019, **62**, 100–107.
- 122 Y. Ma, S. Cheng, X. Wu, Y. Shi, L. Cao, L. Liu, R. Ran, Z. Si, J. Liu and D. Weng, *ACS Catal.*, 2019, **9**, 6962–6973.
- 123 J. Luo, F. Gao, K. Kamasamudram, N. Currier, C. H. F. Peden and A. Yezerets, *J. Catal.*, 2017, **348**, 291–299.
- 124 M. Nielsen, R. Y. Brogaard, H. Falsig, P. Beato, O. Swang and S. Svelle, *ACS Catal.*, 2015, **5**, 7131–7139.
- 125 K. Ehrhardt, M. Suckow and W. Lutz, in *Studies in Surface Science and Catalysis*, Elsevier, 1995, vol. 94, pp. 179–186.
- 126 T. Usui, Z. Liu, H. Igarashi, Y. Sasaki, Y. Shiramata, H. Yamada, K. Ohara, T. Kusamoto and T. Wakihara, *ACS Omega*, 2019, **4**, 3653–3659.
- 127 F. Gao and J. Szanyi, *Appl. Catal., A*, 2018, **560**, 185–194.
- 128 R. Zhang, J.-S. McEwen, M. Kollár, F. Gao, Y. Wang, J. Szanyi and C. H. F. Peden, *ACS Catal.*, 2014, **4**, 4093–4105.
- 129 J. E. Schmidt, R. Oord, W. Guo, J. D. Poplawsky and B. M. Weckhuysen, *Nat. Commun.*, 2017, **8**, 1–8.
- 130 C. Fan, Z. Chen, L. Pang, S. Ming, C. Dong, K. B. Albert, P. Liu, J. Wang, D. Zhu, H. Chen and T. Li, *Chem. Eng. J.*, 2018, **334**, 344–354.
- 131 R. Zhang, Y. Li and T. Zhen, *RSC Adv.*, 2014, **4**, 52130–52139.
- 132 M. Chen, J. Li, W. Xue, S. Wang, J. Han, Y. Wei, D. Mei, Y. Li and J. Yu, *J. Am. Chem. Soc.*, 2022, **144**, 12816–12824.
- 133 Y. Wang, X. Shi, Y. Shan, J. Du, K. Liu and H. He, *Ind. Eng. Chem. Res.*, 2020, **59**, 6416–6423.
- 134 J. M. González and A. L. Villa, *Catal. Lett.*, 2021, **151**, 3011–3019.
- 135 Y. Ma, H. Zhao, C. Zhang, Y. Zhao, H. Chen and Y. Li, *Catal. Today*, 2020, **355**, 627–634.
- 136 L. Sun, M. Yang, L. Cao, Y. Cao, S. Xu, D. Zhu, P. Tian and Z. Liu, *Microporous Mesoporous Mater.*, 2020, **309**, 110585–110595.
- 137 Y. Jangjou, Q. Do, Y. Gu, L.-G. Lim, H. Sun, D. Wang, A. Kumar, J. Li, L. C. Grabow and W. S. Epling, *ACS Catal.*, 2018, **8**, 1325–1337.
- 138 L. Xu, C. Wang, H. Chang, Q. Wu, T. Zhang and J. Li, *Environ. Sci. Technol.*, 2018, **52**, 7064–7071.
- 139 K. Wijayanti, K. Leistner, S. Chand, A. Kumar, K. Kamasamudram, N. W. Currier, A. Yezerets and L. Olsson, *Catal. Sci. Technol.*, 2016, **6**, 2565–2579.
- 140 Y. Jangjou, D. Wang, A. Kumar, J. Li and W. S. Epling, *ACS Catal.*, 2016, **6**, 6612–6622.
- 141 R. Yu, Z. Zhao, S. Huang and W. Zhang, *Appl. Catal., B*, 2020, **269**, 118825–118833.
- 142 Q. Liu, Z. Fu, L. Ma, H. Niu, C. Liu, J. Li and Z. Zhang, *Appl. Catal., A*, 2017, **547**, 146–154.
- 143 X. Li, J. Feng, Z. Xu, J. Wang, Y. Wang and W. Zhao, *React. Kinet., Mech. Catal.*, 2019, **128**, 163–174.
- 144 X. Liu, Y. Li and R. Zhang, *RSC Adv.*, 2015, **5**, 85453–85459.
- 145 C. Yin, P. Cheng, X. Li and R. T. Yang, *Catal. Sci. Technol.*, 2016, **6**, 7561–7568.
- 146 L. Xie, C. Liu, Y. Deng, F. Liu and W. Ruan, *Ind. Eng. Chem. Res.*, 2022, **61**, 8698–8707.
- 147 R. G. Silver, M. O. Stefanick and B. I. Todd, *Catal. Today*, 2008, **136**, 28–33.
- 148 O. Kröcher and M. Elsener, *Appl. Catal., B*, 2008, **77**, 215–227.
- 149 H.-W. Jen, J. W. Girard, G. Cavataio and M. J. Jagner, *SAE Int. J. Fuels Lubr.*, 2009, **1**, 1553–1559.
- 150 I. Lezcano-Gonzalez, U. Deka, H. E. Van Der Bij, P. Paalanen, B. Arstad, B. M. Weckhuysen and A. M. Beale, *Appl. Catal., B*, 2014, **154**, 339–349.
- 151 G. Cavataio, J. R. Warner, J. W. Girard, J. Ura, D. Dobson and C. K. Lambert, *SAE Int. J. Fuels Lubr.*, 2009, **2**, 342–368.
- 152 Y. Kakiuchi, T. Tanigawa, N. Tsunooji, Y. Takamitsu, M. Sadakane and T. Sano, *Appl. Catal., A*, 2019, **575**, 204–213.
- 153 V. Mesilov, S. Dahlin, S. L. Bergman, S. Xi, J. Englund, H. Malm, L. J. Pettersson and S. L. Bernasek, *J. Phys. Chem. C*, 2022, **126**, 3385–3396.
- 154 K. Xie, J. Woo, D. Bernin, A. Kumar, K. Kamasamudram and L. Olsson, *Appl. Catal., B*, 2019, **241**, 205–216.
- 155 A. Wang, K. Xie, D. Bernin, A. Kumar, K. Kamasamudram and L. Olsson, *Appl. Catal., B*, 2020, **269**, 118781–118793.
- 156 N. Zhang, L. Li, Y. Guo, J. He, R. Wu, L. Song, G. Zhang, J. Zhao, D. Wang and H. He, *Appl. Catal., B*, 2020, **270**, 118860–118876.
- 157 W. Hu, F. Gramigni, N. D. Nasello, N. Usberti, U. Iacobone, S. Liu, I. Nova, X. Gao and E. Tronconi, *ACS Catal.*, 2022, **12**, 5263–5274.



- 158 Y. Liu, W. Xue, S. Seo, X. Tan, D. Mei, C. Liu, I.-S. Nam and S. B. Hong, *Appl. Catal., B*, 2021, **294**, 120244–120252.
- 159 H. Lee, I. Song, S. W. Jeon and D. H. Kim, *Catal. Sci. Technol.*, 2021, **11**, 4838–4848.
- 160 H. Lee, R. J. G. Nuguid, S. W. Jeon, H. S. Kim, K. H. Hwang, O. Kröcher, D. Ferri and D. H. Kim, *Chem. Commun.*, 2022, **58**, 6610–6613.
- 161 C. Paolucci, I. Khurana, A. A. Parekh, S. Li, A. J. Shih, H. Li, J. R. Di Iorio, J. D. Albarracin-Caballero, A. Yezerets, J. T. Miller, W. N. Delgass, F. H. Ribeiro, W. F. Schneider and R. Gounder, *Science*, 2017, **357**, 898–903.
- 162 Y. Zhang, J. Zhang, H. Wang, W. Yang, C. Wang, Y. Peng, J. Chen, J. Li and F. Gao, *J. Phys. Chem. C*, 2022, **126**, 8720–8733.
- 163 W. Hu, T. Selleri, F. Gramigni, E. Fenes, K. R. Rout, S. Liu, I. Nova, D. Chen, X. Gao and E. Tronconi, *Angew. Chem., Int. Ed.*, 2021, **60**, 7197–7204.
- 164 W. Hu, U. Iacobone, F. Gramigni, Y. Zhang, X. Wang, S. Liu, C. Zheng, I. Nova, X. Gao and E. Tronconi, *ACS Catal.*, 2021, **11**, 11616–11625.
- 165 K. A. Tarach, M. Jabłońska, K. Pyra, M. Liebau, B. Reiprich, R. Gläser and K. Góra-Marek, *Appl. Catal., B*, 2021, **284**, 119752–119768.
- 166 L. Chen, T. V. W. Janssens, P. N. R. Vennestrøm, J. Jansson, M. Skoglundh and H. Grönbeck, *ACS Catal.*, 2020, **10**, 5646–5656.
- 167 L. Chen, H. Falsig, T. V. W. Janssens and H. Grönbeck, *J. Catal.*, 2018, **358**, 179–186.
- 168 N. Usberti, F. Gramigni, N. D. Nasello, U. Iacobone, T. Selleri, W. Hu, S. Liu, X. Gao, I. Nova and E. Tronconi, *Appl. Catal., B*, 2020, **279**, 119397–119409.
- 169 F. Gramigni, N. D. Nasello, N. Usberti, U. Iacobone, T. Selleri, W. Hu, S. Liu, X. Gao, I. Nova and E. Tronconi, *ACS Catal.*, 2021, **11**, 4821–4831.
- 170 Y. Feng, T. V. W. Janssens, P. N. R. Vennestrøm, J. Jansson, M. Skoglundh and H. Grönbeck, *J. Phys. Chem. C*, 2021, **125**, 4595–4601.
- 171 B. Liu, D. Yao, F. Wu, L. Wei, X. Li and X. Wang, *Ind. Eng. Chem. Res.*, 2019, **58**, 20516–20527.
- 172 L. Wei, D. Yao, F. Wu, B. Liu, X. Hu, X. Li and X. Wang, *Ind. Eng. Chem. Res.*, 2019, **58**, 3949–3958.
- 173 A. J. Shih, J. M. González, I. Khurana, L. P. Ramírez, A. Peña L, A. Kumar and A. L. Villa, *ACS Catal.*, 2021, **11**, 10362–10376.
- 174 J. H. Kwak, D. Tran, J. Szanyi, C. H. F. Peden and J. H. Lee, *Catal. Lett.*, 2012, **142**, 295–301.
- 175 N. Lv, Ch. Sun, X. Wang, Ch. Wang, Y. Yue and X. Bao, *Inorg. Chem. Front.*, 2022, **9**, 1300–1313.
- 176 G. M. Psfogiannakis, J. F. McCleerey, E. Jaramillo and A. C. T. Van Duin, *J. Phys. Chem. C*, 2015, **119**, 6678–6686.
- 177 F. Göttl, A. M. Love and I. Hermans, *J. Phys. Chem. C*, 2017, **121**, 6160–6169.
- 178 J.-S. McEwen, T. Anggara, W. F. Schneider, V. F. Kispersky, J. T. Miller, W. N. Delgass and F. H. Ribeiro, *Catal. Today*, 2012, **184**, 129–144.
- 179 L. Chen, H. Falsig, T. V. W. Janssens, J. Jansson, M. Skoglundh and H. Grönbeck, *Catal. Sci. Technol.*, 2018, **8**, 2131–2136.
- 180 C. Paolucci, A. A. Parekh, I. Khurana, J. R. Di Iorio, H. Li, J. D. Albarracin Caballero, A. J. Shih, T. Anggara, W. N. Delgass, J. T. Miller, F. H. Ribeiro, R. Gounder and W. F. Schneider, *J. Am. Chem. Soc.*, 2016, **138**, 6028–6048.
- 181 S. H. Krishna, C. B. Jones, J. T. Miller, F. H. Ribeiro and R. Gounder, *J. Phys. Chem. Lett.*, 2020, **11**, 5029–5036.
- 182 A. Martini, C. Negri, L. Bugarin, G. Deplano, R. K. Abasabadi, K. A. Lomachenko, T. V. W. Janssens, S. Bordiga, G. Berlier and E. Borfecchia, *J. Phys. Chem. Lett.*, 2022, **13**, 6164–6170.
- 183 C. Negri, T. Selleri, E. Borfecchia, A. Martini, K. A. Lomachenko, T. V. W. Janssens, M. Cutini, S. Bordiga and G. Berlier, *J. Am. Chem. Soc.*, 2020, **142**, 15884–15896.
- 184 A. Oda, H. Shionoya, Y. Hotta, T. Takewaki, K. Sawabe and A. Satsuma, *ACS Catal.*, 2020, **10**, 12333–12339.
- 185 R. Daya, D. Trandal, U. Menon, D. J. Deka, W. P. Partridge and S. Y. Joshi, *ACS Catal.*, 2022, **12**, 6418–6433.
- 186 T. Zhang, H. Chang, Y. You, C. Shi and J. Li, *Environ. Sci. Technol.*, 2018, **52**, 4802–4808.
- 187 T. Yu, J. Wang, Y. Huang, M. Shen, W. Li and J. Wang, *ChemCatChem*, 2014, **6**, 2074–2083.
- 188 M. Jabłońska and R. Palkovits, *Appl. Catal., B*, 2016, **181**, 332–351.
- 189 L. Chmielarz and M. Jabłońska, *RSC Adv.*, 2015, **5**, 43408–43431.
- 190 M. Jabłońska, *Molecules*, 2021, **26**, 6461–6485.
- 191 K. Leistner, O. Mihai, K. Wijayanti, A. Kumar, K. Kamasamudram, N. W. Currier, A. Yezerets and L. Olsson, *Catal. Today*, 2015, **258**, 49–55.
- 192 L. Olsson, K. Wijayanti, K. Leistner, A. Kumar, S. Y. Joshi, K. Kamasamudram, N. W. Currier and A. Yezerets, *Appl. Catal., B*, 2015, **174**, 212–224.
- 193 J. Guo, W. Yang, Y. Zhang, L. Gan, C. Fan, J. Chen, Y. Peng and J. Li, *Catal. Commun.*, 2020, **135**, 105751–105756.
- 194 M. Jabłońska and A. Mollá Robles, *Materials*, 2022, **15**, 4770–4794.
- 195 H. Wang, R. Xu, Y. Jin and R. Zhang, *Catal. Today*, 2019, 295–307.
- 196 S. Shrestha, M. P. Harold, K. Kamasamudram, A. Kumar, L. Olsson and K. Leistner, *Catal. Today*, 2016, **267**, 130–144.
- 197 P. S. Dhillon, M. P. Harold, D. Wang, A. Kumar and S. Y. Joshi, *Catal. Today*, 2021, **360**, 426–434.
- 198 P. S. Dhillon, M. P. Harold, D. Wang, A. Kumar and S. Y. Joshi, *React. Chem. Eng.*, 2019, **4**, 1103–1115.
- 199 Y. Liao, H. Xu, Z. Li, L. Ji, L. Wang, G. Gao, W. Huang, Z. Qu and N. Yan, *J. Phys. Chem. C*, 2021, **125**, 17031–17041.
- 200 A. K. Datye and M. Votsmeier, *Nat. Mater.*, 2021, **20**, 1049–1059.

